Spatial confinement and temporal dynamics of selectin ligands enable stable hematopoietic stem cell rolling

Bader Al Alwan[1,4], Karmen AbuZineh[1], Shuho Nozue[1], Aigerim Rakhmatulina[1], Mansour Aldehaiman[1], Asma S. Al-Amoodi[1], Maged F. Serag[1], Fajr A. Aleisa[1], Jasmeen S. Merzaban[1,2,*] and Satoshi Habuchi[1,2,3,*]

[1] King Abdullah University of Science and Technology (KAUST), Biological and Environmental Science and Engineering Division, Thuwal 23955-6900, Saudi Arabia

[2] These authors contributed equally to the work

[3] Lead contact

[4] Current address: Stem cell and Regenerative medicine-King Abdullah International Medical Center (KAIMRC) – Kind Saud bin Abdulaziz University for Health Sciences

*Correspondence should be addressed to S.H. (King Abdullah University of Science and Technology (KAUST), Biological and Environmental Sciences and Engineering Division, Thuwal 23955-6900, Saudi Arabia. E-mail: Satoshi.Habuchi@kaust.edu.sa), or J.S.M. (King Abdullah University of Science and Technology (KAUST), Biological and Environmental Sciences and Engineering Division, Thuwal 23955-6900, Saudi Arabia. E-mail: Jasmeen.Merzaban@kaust.edu.sa)

Summary

Hematopoietic stem/progenitor cell (HSPC) homing is initiated by tethering and rolling of the cells on endothelium through selectin-ligand interactions. Although multiple factors that affect the rolling behavior of the cells have been identified, molecular mechanisms that enable slow and stable cell rolling remain elusive. Here, using a microfluidics-based single-molecule live cell fluorescence imaging, we reveal that unique spatiotemporal dynamics of selectin ligands on the membrane tethers and slings, which are distinct from that on the cell body, play an essential role in the rolling of the cell. Our results suggest that the spatial confinement of the selectin ligands to the tethers and slings together with the rapid scanning of a large area by the selectin ligands increases the efficiency of selectin-ligand interactions during cell rolling, resulting in slow and stable rolling of the cell on the selectins. Our findings provide novel insights and contribute significantly to the molecular-level understanding of the initial and essential step of the homing.

Keywords

Selectin ligands, single-molecule imaging, PSGL-1, CD44, E-selectin, membrane tethers, microvilli, diffusion, lipid rafts, actin cytoskeleton

Introduction

Delivering circulatory cells to specific sites in the body is central to many physiological functions, from immunity to cancer metastasis, which is achieved by their interactions with the surface of endothelium under the presence of external shear forces (Ley et al., 2018; Quail and Joyce, 2013). These cellular interactions are controlled by a number of adhesion molecules that include selectins and integrins and their corresponding ligands (Kolaczkowska and Kubes, 2013). So far, molecular mechanisms of cell adhesion have been investigated by characterizing migration behavior at the cellular level in the presence of shear force exerted to the migrating cells and/or characterizing binding behavior of the adhesion molecules with their ligands at the molecular level by applying external force to the bonds using, for example, single-molecule force spectroscopy technique (Alon et al., 1995; Marshall et al., 2003; McEver and Zhu, 2010). However, under physiological flow conditions, interactions between adhesion molecules and their ligands occur under a spatiotemporal rather heterogeneous cellular environment. Thus, without capturing real-time nanoscopic spatiotemporal interactions of adhesion molecules and their ligands at the molecular level in the cellular environment, one cannot develop a complete picture of complicated cellular interactions that exist.

Hematopoietic stem/progenitor cell (HSPC) homing is an important biological phenomenon in which transplanted HSPCs travel from peripheral blood to the bone marrow (Magnon and Frenette, 2008). The homing of HSPCs to bone marrow is a multistep process that is initiated by tethering and rolling of the cells on endothelium (Ley et al., 2007; Magnon and Frenette, 2008; McEver and Zhu, 2010; Sundd et al., 2013). The initial step of homing is mediated by the binding of homing receptors expressed on endothelial cells, E- and P-selectin (Lehr and Pienta, 1998; Schweitzer et al., 1996), to their ligands expressed on the HSPCs that include CD44

(Dimitroff et al., 2001; Ponta et al., 2003) and PSGL-1 (Goetz et al., 1997; Yago et al., 2010a). HSPCs are tethered to the endothelium by the selectin-ligand interactions resulting in their rolling along the endothelium at shear stress of several dynes cm^{-2} generated by the blood flow (Frenette et al., 1998; Hidalgo et al., 2002; Mazo et al., 1998). Although multiple factors that affect the rolling behavior of the cells have been identified, including spatial clustering of the ligands (Abbal et al., 2006), formation of membrane tethers and slings (Sundd et al., 2012), and shear force-dependent selectin-ligand interactions (Marshall et al., 2003), spatiotemporal dynamics of selectin ligands during this initial step of homing and its contribution to slow and stable cell rolling are not well understood. This is due the lack of an experimental method that enables capturing real-time nanoscopic spatiotemporal interactions of adhesion molecule and their ligands at the molecular level in the cellular environment.

In this study, using a microfluidics-based single-molecule live cell fluorescence imaging technique, we showed that the unique spatiotemporal dynamics of selectin ligands on the membrane tethers and slings play an essential role in the rolling of the cell. We demonstrated that the membrane tethers are formed from single microvilli on the cells and this provides a mechanism to spatially localize selectin ligands, in particular PSGL-1 and CD44, on these tethers and slings. Furthermore, this work also established that due to the detachment of the cell from the actin cytoskeleton during the formation of the tethers, fast and random diffusional motion of selectin ligands is exhibited along these structures (i.e., tethers and slings) in contrast to the slow and confined motion of the ligands on the cell body. Our results suggest that the spatial confinement of the selectin ligands to the tethers and slings together with the rapid scanning of a large area by the selectin ligands increases the efficiency of selectin-ligand interactions during cell rolling, resulting in slow and stable rolling of the cell on the selectins.

Results

Experimental design

We developed a microfluidics-based single-molecule fluorescence imaging platform to capture and characterize molecular level spatiotemporal dynamics of selectin ligands that occur during cell rolling on selectins (AbuZineh et al., 2018). To this end, we deposited recombinant human (rh) E-selectin on the surface of a microfluidic chamber (Figure S1A) at the surface density of 0.6 – 111 molecules μm^2. A suspension of primary human $CD34^{pos}$-HSPCs or KG1a cells, a human leukemic progenitor cell line often used as a model system of HSPCs (AbuSamra et al., 2015; AbuSamra et al., 2017; Merzaban et al., 2011), were injected into the fluidic chamber at the shear stresses of 1 – 8 dyne cm^{-2} using a syringe pump (Figure 1A). The number of bound cells to the surface E-selectin increased with the increase of the surface density of E-selectin (Figure S1B), whereas the rolling velocity of the cells decreased with the increase of the surface density (Figure S1C). We observed that the binding of the cells to E-selectin requires calcium ion (Figure S1D). All these observations suggest that the tethering and rolling of the cells are caused by the specific interaction between the selectin ligands on the cells and the surface E-selectin, mimicking in vivo cell rolling behavior.

The cytoplasmic membrane of the primary human $CD34^{pos}$-HSPCs and KG1a cells was fluorescently-stained using Vybrant DiO dye. CD44 and PSGL-1, two selectin ligands expressed on these cells were immunolabeled by fluorophore (either Alexa-Fluor-488, Alexa-Fluor-555, or Alexa-Fluor-647)-conjugated antibodies (515 mAB and KPL-1 mAB for CD44 and PSGL-1, respectively) and introduced into the chamber. Fluorescence-activated cell sorting (Figure 1B and S1E) and fluorescence imaging of labeled cells (Figure 1C) was used to confirm the binding

specificity of these antibodies. Since antibodies have two binding sites to their epitopes that may cause artificial clustering of the labeled molecules, we immunostained PSGL-1 on KG1a cells using the Alexa-Fluor-555-conjugated Fab fragment of the anti-PSGL-1 antibody (Alexa-555-Fab) that has only one binding site to its epitope. The immunofluorescence image of PSGL-1 on the membrane tethers and slings of the KG1a cells (see below) obtained using the Alexa- 555-Fab showed a spatial distribution of the PSGL-1 molecules very similar to that obtained using the Alexa-Fluor-555-conjugated anti-PSGL-1 antibody (Figure 1D). This result demonstrates that the spatial distribution of the selectin ligands on the cells are not the result of artificial clustering of PSGL-1 due to the bivalency effect of the antibody.

Visualization of membrane tethers/slings and selectin ligands

A standard 2D epi-fluorescence microscopy images of the Vybrant DiO-stained KG1a cells rolling on E-selectin at a shear stress of 2 dyne cm^{-2} illustrated the formation of membrane tethers and slings (Figure 1E) (Sundd et al., 2012). Membrane tethers that appear during cell rolling on selectins are believed to play a critical role in the stable rolling of the cells. Previous studies demonstrated that live cells roll on a selectin surface more stably compared to fixed cells or to microspheres coated with selectin ligands (Sundd et al., 2013). These observations suggest that tethers help decrease the tension exerted on selectin-ligand bonds and thereby reduce the probability of breaking these interactions. This stronger binding is consistent with previous studies from our lab illustrating that the off rate of binding between selectin ligands and E-selectin is low (AbuSamra et al., 2015; AbuSamra et al., 2017). Two-color epi-fluorescence imaging of the cell membrane and CD44 of the KG1a cells showed perfect colocalization of the two images, demonstrating that the tethers and slings can also be visualized by the immunofluorescence image

of the CD44 molecules (Figure 1E). Using the immunofluorescence images of CD44, we confirmed that the membrane tethers and slings are formed on the $CD34^{pos}$-HSPCs during the cell rolling in a way similar to those formed on the KG1a cells (Figure 1F).

To fully visualize the formation of the tethers and slings during cell rolling along with the spatial distributions of the selectin ligands on the tethers and slings, we reconstructed 3D fluorescence images of CD44 and PSGL-1 on the rolling KG1a cells by recording epi-fluorescence images of the specimens at different Z-axis positions with 0.5 – 1.0 μm step size (Figure 1A). Due to the fluorescence from out-of-focus regions, the reconstructed 3D fluorescence images of the cell body are distorted along the Z-axis and fine structures on the cell body cannot be resolved clearly. On the other hand, the width of the membrane tethers and slings formed during the cell rolling (see below) captured by the fluorescence images of CD44 and PSGL-1 is close to the diffraction-limited size defined by the Rayleigh criterion (0.21 – 0.33 μm in our experimental conditions). The depth of filed (Z) in our experimental conditions is calculated by using the following equation (Murphy and Davidson, 2012)

$$Z = \frac{n\lambda}{\mathrm{NA}^2}, \quad (1)$$

where n is the refractive index of the medium between the objective lens and the specimen. λ and NA denote the wavelength of light (i.e. fluorescence wavelength) and the numerical aperture of the objective lens. Given the optical characteristics of the objective lenses (n = 1.51, NA = 1.49 for UAPON 100XOTIRF and n = 1.41, NA = 1.25 for UPLSAPO40XS) and the spectroscopic properties of the fluorophores (λ = 0.5 – 0.67 μm) used in this study, the depth of field in our experiments is estimated to be in the range of 0.34 – 0.60 μm. Since the physical size (i.e. width and depth) of the tethers and slings is smaller than the depth of field, our imaging mode enables to reconstruct the 3D image of the tethers and slings at the spatial resolution defined by the depth of

field without the effect of out-of-focus fluorescence (Figure 1I). 2D fluorescence images were captured using standard epi-illumination wide-field fluorescence microscopy. The spatiotemporal dynamics of the selectin ligands on the tethers and slings were captured at the single-molecule level by either 2D (Figure 1G and 1H) or 3D epi-illumination wide-field fluorescence microscopy (Figure 1I and 1J) in a way similar to the visualization of the tethers and slings.

Spatiotemporal dynamics of tethers and slings

The tethers and slings were formed on KG1a cells at all the shear stresses used in this study (1 – 8 dyne cm^{-2}, Figure 2A and S2A, Video S1). The formation of the tethers and slings was also observed for primary human $CD34^{pos}$-HSPCs at a shear stress of 2 dyne cm^{-2} (Figure 1F). These are in contrast to the previous study on neutrophils rolling over P-selectin, which showed the formation of the tethers and slings only at shear stresses higher than 6 dyne cm^{-2} (Sundd et al., 2012). The length of the tethers and slings range in size between several micrometers to tens of micrometers (Figure 2B, S2B and S2C). The mean lengths of the tether and sling increased from 18 to 30 μm and from 13.5 to 30 μm for the tethers and slings, respectively when the applied shear stress was increased from 1 to 8 dyne cm^{-2} (Figure 2B). Interestingly, on occasion, tethers and slings longer than 100 micrometers were observed (Figure 2B). Time-lapse fluorescence images of CD44 clearly demonstrated that a tether detached from the E-selectin surface is converted into a sling within several hundreds of milliseconds in both KG1a cells and primary human $CD34^{pos}$-HSPCs (Figure 2C and S2D, Video S2) (Marki et al., 2016). Given that the primary human $CD34^{pos}$-HSPCs showed very similar structures to our model $CD34^{pos}$ cell line and that access to these primary cells is limited, we chose to focus on KG1a cells for all subsequent experiments. While the slings are persistent structures, we also observed a retraction

of the slings during cell rolling (Figure 2D, Video S3). The side views of the 3D images visibly show the formation of multiple tethers and slings during cell rolling over E-selectin (Figure 1I). In addition, the time-lapse 3D images captured the elongation of tethers (Figure 2E) and change in the Z-axis position of the slings (Figure 2F) during cell rolling. We also often observed the formation of anchoring points on the tethers (Figure 1G and 2G).

Spatial clustering of selectin ligands at tethering and anchoring points

The immunofluorescence images of CD44 on KG1a cells showed the contiguous distribution of CD44 on the tethers and slings (Figure 1G). In contrast, we found that PSGL-1 shows a discrete spatial distribution on the tethers and slings (Figure 1H and 1J, Video S4 and S5). The PSGL-1 molecules on the tethers and slings displayed perfect spatial overlap with the cell membrane and CD44 (Figure 3A and 3B). The side views of the 3D images also unambiguously demonstrated that the tethers and slings are entirely covered with the CD44 and PSGL-1 molecules in a distinct spatial distribution (i.e. contiguous and discrete distributions for CD44 and PSGL-1, respectively, Figure 3C and 3D). These results demonstrated that the entire tethers were consistently covered by the selectin ligands during their elongation (Figure 1I and 1J).

The fluorescence images of CD44 and PSGL-1 on the tethers and slings sometimes show bright spots at their tips (Figure 3C, 3D and S4), indicating clustering of the selectin ligands at the tethering points. The clustering of selectin ligands at the tethering points was further investigated by calculating the number of PSGL-1 molecules at each spot on the tethers and slings. Our calculation demonstrated that each PSGL-1 spot distributed on the tethers and slings mainly corresponds to a single PSGL-1 molecule (Figure 3E). The distributions can be fitted to Poisson distribution using the following equation

$$y = e^{-r}\frac{r^x}{x!}\ , \qquad (2)$$

where r is the mean of the distribution (Figure 3E). This result indicates that the number of PSGL-1 molecules in each spot on the tethers and slings is determined in a stochastic way with the mean number of one PSGL-1 molecule per spot. Since the fluorescence labeling of the antibodies by the Alexa-Fluor-dyes also has as stochastic nature (i.e. each antibody carries a different number of the Alexa-Fluor-dyes whose distribution is described by Poisson distribution), the obtained Poisson distribution of the number of PSGL-1 molecules in each spot on the tethers and slings could be affected by this. However, the degree of labeling is in the range of 4 – 8 dyes per antibody, which should not give the experimentally observed Poisson distribution (i.e. mean number of one). Given the one-to-one binding of the antibody and PSGL-1, the result rather suggests that the number of PSGL-1 molecules in each spot on the tethers and slings is indeed determined in a stochastic way (i.e. absence of a mechanism that colocalizes the PSGL-1 molecules together) with the mean number of one PSGL-1 molecule per spot.

In contrast to the distributions of PSGL-1 on the tethers and slings, we found that multiple PSGL-1 molecules are present at the tethering point (4.1 molecules, Figure 3E) and anchoring point (2.3 molecules, Figure 3E), suggesting the spatial clustering of the selectin ligands at the tethering and anchoring points. The frequency histograms of the number of the PSGL-1 molecules in each spot at the tethering points (Figure 3E) and anchoring points (Figure 3E) show a significant deviation from Poisson distribution. The result suggests that the number of PSGL-1 molecules in each tethering and anchoring point is not determined in a stochastic way. Instead, the result suggests the presence of a specific mechanism that supports the spatial clustering of PSGL-1 in the tethering and anchoring points.

Spatial clustering of selectin ligands supports the tethers/slings formation

To investigate the effect of the clustering of the selectin ligands on the formation of tethers/slings and on the rolling behavior of the cell, we disrupted the clusters of CD44 by treating the cells with methyl-β-cyclodextrin (MβCD) (Abbal et al., 2006; AbuZineh et al., 2018; Setiadi and McEver, 2008). Cholesterol existing in the cell membrane is extracted by this treatment, leading to the disruption of lipid rafts domains. Super-resolution fluorescence localization microscopy images of CD44 on the KG1a cells clearly showed that the 200 nm-size CD44 clusters existing on the control cells are disrupted by the MβCD treatment (Figure 3F and 3G) (AbuZineh et al., 2018). Scanning electron microscopy (SEM) images of the control and MβCD-treated KG1a cells clearly revealed that microvilli existing on the control cells (Figure 3H and S5A) disappear upon the MβCD treatment (Figure 3I and S5B). These results are reminiscent of previous data from our lab showing that CD34 plays a key role in the formation of microvilli structures since once they are knocked down, microvilli structures disappear (AbuSamra et al., 2017). This result strongly suggests that the CD44 molecules localize on the microvilli in the control cells.

The two-color fluorescence imaging experiment of the membrane stain and CD44 on the MβCD-treated KG1a cells showed perfect spatial colocalization of CD44 and the cell membrane in the tethers and slings (Figure 3J), confirming that the spatiotemporal behavior of the tethers and slings on the MβCD-treated cells can be characterized by analyzing fluorescence images obtained for CD44. We found that the formation of the tethers and slings is extremely inefficient under the MβCD-treated condition (Figure 3K) as well as when CD34 is knocked down (Figure 3L and S6). While the tethers and slings are formed in more than 90 % of the control cells rolling over E-selectin (Video S6), they are observed in less than 10 % of the MβCD-treated cells and CD34 knockdown cells. Further, the length of the tethers and slings formed during the rolling of

the MβCD-treated cells were much shorter than those formed in the control cells (Figure 3M). The fluorescence images of CD44 on the MβCD-treated cells and CD34 knockdown cells never showed bright spots (i.e. clusters of CD44) at the tethering points (Figure 3K and 3L). These results demonstrate that the clustering of the selectin ligands contributes to both initial binding to the surface E-selectin (i.e. tether formation) as well as the elongation of the tethers against the tension exerted to the tethering point during cell rolling. Our finding also suggests that the microvilli play a key role in the spatial clustering of the selectin ligands and the formation of the tethers and slings during cell rolling over E-selectin.

Selectin ligands are spatially confined to the tethers and slings

Based on these findings, we next sought to investigate the mechanism of the formation of the tethers. To that end, we calculated the total number of the PSGL-1 molecules on a single tether during its elongation (Figure 4A). The time lapse images of PSGL-1 showed that the integrated fluorescence intensity per unit length (i.e. number density of the PSGL-1 molecules along the tether) decreases (Figure 3B) during the elongation of the tether (Figure 3C), whereas the integrated intensity over the entire tether (i.e. total number of the PSGL-1 molecules on the tether) is almost constant during the tether elongated from 75 μm to 110 μm (Figure 3D).

We also calculated the mean total number of the PSGL-1 molecules on single tethers and slings at different shear stresses (Figure 3F) using the mean lengths of the tethers/slings (Figure 2B and 3G) and the mean distances between the adjacent PSGL-1 molecules on the tethers/slings at different shear stresses (Figure 3E and 3H). We found that both the mean lengths and distances increased with the increase of the applied shear stresses (Figure 3G and 3H). The calculated mean total number of the PSGL-1 molecules on single tethers and slings clearly showed that the

number is almost constant over the 1 – 8 dyne cm^{-2} although the tethers and slings were two times longer at 8 dyne cm^{-2} compared with those at 1 dyne cm^{-2} (Figure 3F). The density of CD44 molecules on the tethers and slings also decreased with an increase in the shear stress (i.e. larger distances between the adjacent CD44 molecules on the tethers/slings at higher shear stresses, Figure 3I), similar to PSGL-1 on the tethers and slings.

Given the localization of PSGL-1 and CD44 on the microvilli (Abbal et al., 2006; AbuZineh et al., 2018; Miner et al., 2008; Moore et al., 1995), our results strongly suggest that single tethers and therefore slings are formed from single microvilli upon their binding to the surface E-selectin. This is supported by our observation that the tethers and slings are always covered entirely by CD44 and PSGL-1 (Figure 1E and 3B). If the tethers are formed from multiple microvilli, this would result in discrete patches of CD44 and PSGL-1 clusters on the tethers and slings.

Selectin ligands on the tethers and slings show fast and random diffusion

Single-molecule imaging revealed that the PSGL-1 molecules show diffusional motion on the tethers and slings (Figure 5A, Video S4 and S5). We analyzed their motion using mean square displacement (MSD) analysis of the single-molecule diffusion trajectories (Figure 5B, S7A and S7B). The MSD analysis showed that the PSGL-1 molecules on the tethers have a mean diffusion coefficient of approximately 0.17 $\mu m^2 s^{-1}$ (Figure 5C, S7C and S7D). The single-molecule tracking analysis of the PSGL-1 molecules on the slings could be affected by the motion of the slings (i.e. either stable or retracting) and the cell (i.e. either rolling within the acquisition time of the diffusion trajectory or not). Thus, we split the diffusion trajectories into three categories and calculated the mean square displacement (MSD) versus time lag plots

separately; PSGL-1 molecules diffusing on the stable slings without the effect of the cell rolling, pSGL-1 molecules diffusing on the retracting slings without the effect of the cell rolling, and PSGL-1 molecules diffusing on the stable slings with the effect of the cell rolling. While we observed slight differences between the three cases, in principle, all the MSD versus time lag plots showed linear relationship with a mean diffusion coefficient of approximately 0.21 $\mu m^2 s^{-1}$ (Figure 5B and 5C). The effect of the retraction of the slings and the cell rolling is negligible in our MSD analysis because of the decoupling of the time scale of the diffusional motion of the PSGL-1 molecules and the motion of the slings and the cells. The observed diffusion coefficients of the PSGL-1 molecules on the tethers and slings are much faster than those reported for membrane proteins including PSGL-1 on neutrophils (0.003 $\mu m^2 s^{-1}$) (Gaborski et al., 2008). The MSD analysis also demonstrated that the PSGL-1 molecules display random diffusion on the tethers and slings (i.e. linear relationship between the MSD and time lag, Figure 5B).

We also conducted single-molecule tracking experiments of the PSGL-1 molecules on the control cells (i.e. localized on microvilli) (Figure 5D). The experiment was conducted by placing the immunostained cells on the surface of the microfluidic chamber. Although we did not deposit any molecules that have a specific interaction with the PSGL-1 molecules (e.g. E-selectin), the PSGL-1 molecule may interact with the surface in a nonspecific manner, and therefore the diffusional motion of the PSGL-1 may be affected. Thus, we analyzed the single-molecule diffusion trajectories obtained from both the bottom and top surfaces of the cells. The MSD versus time lag plots obtained from these experiments showed very similar behavior (Figure 5E), confirm that there is a negligible effect of the surface on the diffusional motion of the PSGL-1 molecules localized on microvilli. The MSD analysis of the diffusion trajectories showed that the PSGL-1 molecules on the control cells diffuse much slower than those distributing on the tethers

and slings (i.e. mean diffusion coefficient of 0.10 and 0.094 $\mu m^2 s^{-1}$ for the top and bottom surfaces of the cells, respectively, Figure 5C). The analysis also revealed that the PSGL-1 molecules on the control cells show a confined diffusion with a confinement area of 0.32 and 0.29 μm^2 for the top and bottom surfaces of the cells, respectively (Figure 5F and S7E).

Actin cytoskeleton detaches from the cell membrane during the tethers/slings formation

We found that multiple tethers sometime merged into a single tether during cell rolling (Figure 6A, Video S7), which occurs within a second. Together with the larger motional freedom (i.e. faster and random diffusion) of the PSGL-1 molecule on the tethers and slings compared with those localized to the microvilli, these observations imply the involvement of the actin cytoskeleton in the spatiotemporal dynamics of the tethers and slings. We thus conducted a two-color fluorescence imaging experiment of CD44 (labeled by either Alxa-Fluor-488- or Alxa-Fluor-647-conjugated antibodies) and actin (labeled by either silicon-rhodamine-conjugated jasplakinolide (Lukinavicius et al., 2014) or Alexa-Fluor-488-conjugated phalloidin). The fluorescence image of CD44 and actin on the control KG1a cells showed perfect colocalization (Figure 6B). On the other hand, we did not observe any fluorescence signal of actin from the tethers and slings in most cells rolling over E-selectin. In some rare cases, we found that actin exists along the tethers and slings of the rolling cells, but in a form of small fragmented patches (Figure 6C). This result unambiguously demonstrates that the cell membrane is detached from the cortical actin cytoskeleton during the formation of the tethers, consistent with previous force spectroscopy studies that indicated the detachment (Evans et al., 2005; Heinrich et al., 2005; Shao et al., 1998).

Discussion

Formation of tethers and slings

In this study, we were able to captured real-time spatiotemporal behavior of the tethers and slings by capturing the very bright and contiguous fluorescence of CD44 on the tethers and slings (Figure 2C). Our live-cell fluorescence imaging experiment clearly captured the flipping of the broken tethers from the rear side of the KG1a cell to its front side during rolling on E-selectin (Figure 2C). The images demonstrate that the flipping of the tethers occurred at a time scale of approximately 240 ms. This time scale is longer than that reported for neutrophils rolling on P-selectin (less than 100 ms (Marki et al., 2016)), although similar tethers and slings were observed in both cell types. Given much larger shear stress (10 dyne cm^{-2}) used in the experiment on neutrophils compared with our experiment (Figure 2C, 6 dyne cm^{-2}), the observed difference is likely to be due to the different flow velocities in these experiments rather than different elastic properties of the tethers formed in these experiments. These results indicate that the elastic properties of the tethers and slings that make these structures so flexible are similar in different cell types, implying the existence of common mechanisms in the formation of tethers and slings.

We observed the formation of the tethers with mean lengths of 18 – 30 μm at shear stresses ranging between 1 and 8 dyne cm^{-2} (Figure 4G). Although the formation of tethers has been reported for neutrophils rolling over P-selectin (Sundd et al., 2012), relatively short tethers (mean lengths of approximately 10 μm) were observed only at high shear stresses (above 6 dyne cm^{-2}) (Marki et al., 2016). Although we cannot rule out the possibility that cell type dependent elastic properties of cell membranes may affect the tethering behavior, it is more likely that the difference is due to the strength of selectin-ligand interactions. Our observations suggest that E-

selectin-ligand interactions are much stronger than P-selectin-ligand interactions. Since rapture force of E-selectin-ligand interactions observed for polymorphonuclear leukocytes is similar to that of P-selectin-ligand interactions (Hanley et al., 2004), it is likely that the difference in the binding strength between E-selectin and P-selectin is a result of different dissociation constants against their ligands. This is supported by our finding that KG1a cells roll faster over the P-selectin surfaces than E-selectin surfaces. The stronger binding (i.e. smaller dissociation rate) of the tethers resists shear stresses for longer periods of time before they dissociate from the surface selectins, and thus causes the formation of longer tethers. This stronger binding is consistent with previous studies from our lab illustrating that the k_{off} of binding between selectin ligands and E-selectin is low (AbuSamra et al., 2015; AbuSamra et al., 2017).

Spatial clustering of selectin ligands promotes the formation of tethers and slings

We found that the PSGL-1 molecules show discrete distribution along the tethers and slings mostly as single molecules (Figure 3E). Importantly, we observed larger numbers of PSGL-1 molecules at the tethering points (on average 4.1 molecules, Figure 3E) and the anchoring points (on average 2.3 molecules, Figure 3E). Although it is still controversial (Hocde et al., 2009; Snapp et al., 2002), PSGL-1 molecules are believed to localize to the tip of microvilli in order to facilitate efficient binding of PSGL-1 to selectins (Abbal et al., 2006; Miner et al., 2008; Moore et al., 1995). Previous work from our lab also suggested the localization of CD44 to the microvilli of the cells (AbuZineh et al., 2018). Our findings in this study, in principle, agree with this model that the spatial confinement of the selectin ligands to microvilli enhances the probability that multiple ligand molecules in the confined area bind to P- or E-selectin on the surface, which leads to the formation of a tether against the tension exerted to the tethering point.

Simulation studies suggested that spatial clustering of ligands strengthens ligand-receptor interactions (Gopalakrishnan et al., 2005) and helps cells to roll stably on a selectin surface (Schmidt et al., 2009). While these studies did not consider the formation of the tethers and slings, the critical role of the spatial clustering of selectin ligands in the cell rolling reported in the study is consistent with our observation.

Our findings demonstrated that the larger numbers of the PSGL-1 molecules exist at the tethering points compared with those at anchoring points. Since the anchoring points are formed after the initial tethering events occur, the tension exerted to the anchoring points should be smaller than that exerted to the tethering points. Thus, the smaller numbers of PSGL-1 at the anchoring points is an indication that the initial tether formation requires the binding of multiple PSGL-1 molecules to the surface E-selectins, which enables to resist high tension exerted to the tethering points. Note that we don't know yet if these anchoring points are formed at the rear side of the cells during the formation of the tethers. They may be formed during the sling binding to the surface at the front side of the cells as suggested by a previous study (Sundd et al., 2012).

Since CD34 knockdown KG1a cells (AbuSamra et al., 2017) and MβCD-treated KG1a cells (AbuZineh et al., 2018) exhibit approximately 3-5 times faster rolling velocity compared with control cells and showed more unstable rolling (i.e. faster detachment) on E-selectin, our findings suggest that the efficient formation of the tethers and slings and their strong resistance to shear stress due to the spatial clustering of the selectin ligands on the microvilli enables the slow and stable rolling of the cells. Data from our lab has shown that the binding of E-selectin to its ligands is limited by a slow-on rate (AbuSamra et al., 2015; AbuSamra et al., 2017) and this observation that clustering of the ligands (i.e. CD44 and PSGL-1) occurs at anchor points helps

to explain how the cell in flow can overcome this “slow on” rate and enhance the binding of E-selectin to its ligands ultimately through the increase in the local concentration of the ligands.

Spatial confinement of selectin ligands to tethers and slings promotes stable cell rolling

Previous studies suggested that PSGL-1 molecules localize to a tip of microvilli by their association with lipid rafts (Miner et al., 2008; Shao et al., 2015; Yago et al., 2010b) and actin binding proteins (ezrin/radixin/moesin (ERM) proteins) (Miner et al., 2008; Snapp et al., 2002). Our single-molecule imaging experiments revealed that PSGL-1 molecules distribute along the entire tethers and slings (Figure 3B). This result suggests that these subcellular structures are disrupted during the formation of the tethers.

Previous studies suggested that the localization of selectin ligands to microvilli enables them to interact with selectins during the initial step of homing (Miner et al., 2008; Moore et al., 1995). Our findings here extend this to the tethers and slings (Figure 7A). During cell rolling, CD44 and PSGL-1 are spatially redistributed to the entire tethers and slings by the conversion of single microvilli to the tethers. This redistribution significantly increases the exposure of these selectin ligands to the surface E-selectin, promoting clustering and efficient selectin-ligand binding that leads to mechanisms that help overcome the slow-on rate (AbuSamra et al., 2015; AbuSamra et al., 2017) leading to slow and stable rolling.

Fast diffusion of selectin ligands on tethers and slings promotes stable cell rolling

The diffusion coefficient of the PSGL-1 molecules localized on the microvilli of the control KG1a cells obtained from the MSD analysis (0.1 $\mu m^2 s^{-1}$) is approximately 30 fold larger than the diffusion coefficient of PSGL-1 reported previously using fluorescence recovery after

photobleaching (FRAP) technique (0.003 $\mu m^2 s^{-1}$) (Gaborski et al., 2008). Given the different time and length scales of the diffusional motion captured by these two methods, it is very likely that we captured the motion of microvilli rather than the diffusional motion of the PSGL-1 molecules in our single-molecule fluorescence imaging experiment (i.e. the PSGL-1 molecules stay at the tip of microvilli during the image acquisition and therefore we capture the motion of the microvilli through the fluorescence signal of the PSGL-1 molecules) (Cai et al., 2017). This is strongly supported by the fact that the size of the confinement area (0.3 μm^2 that corresponds to the confinement length of approximately 0.54 μm) estimated by the MSD analysis is close to the size of the area expected to be covered by the microvilli since our SEM experiments on the KG1a cells revealed that the length of the microvilli is in the range of several hundred of nanometers (Figure 3H). Also, the length of the microvilli on neutrophils has been estimated to be about 0.3 μm (Shao et al., 1998). Therefore, the real diffusion coefficient of the PSGL-1 molecules localized on the microvilli would be much smaller than our estimation by the MSD analysis of the single-molecule diffusion trajectories and may be closer to the value determined by the FRAP technique. The difference in the diffusion coefficient obtained in our experiment and in the previous study may also be partly explained by differences from cell to cell.

Since PSGL-1 and CD44 on the control cells are directly or indirectly anchored to the actin cytoskeleton in the microvilli by actin binding ERM proteins (Moore et al., 1995; Snapp et al., 2002; Wang et al., 2014), the formation of the tethers and therefore the detachment of the membrane from the actin cytoskeleton would cause a significant enhancement in the motional freedom of PSGL-1 and CD44, consistent with the results obtained from the single-molecule tracking analysis (Figure 7B). Due to the distinct rates and modes of the diffusion, the PSGL-1 molecules on the tethers and slings cover much larger displacement areas compared with those

restricted to the microvilli (0.14 μm^2 and 0.26 μm^2 for tethers and slings, respectively compared with 0.038 μm^2 for microvilli) during the several hundreds of milliseconds of the lifetime of the tethers (Chen and Springer, 1999; Schmidtke and Diamond, 2000). The difference becomes even larger when more stable structures (i.e. tethers with multiple anchoring points and non-retracting slings that exist for more than several seconds) are formed during cell rolling.

To form a selectin-ligand bond, the ligand molecules on the rolling cell have to be located within tens of nanometers distance from the surface E-selectin molecules (Cummings and McEver, 2009). If the locations of the PSGL-1 molecules are fixed, the probability to find the surface E-selectin molecules within this distance is relatively low. Thus, the fast and random motion of the selectin ligands on the tethers and slings, which enables them to scan large surface area during a limited lifetime of tethers (with anchoring points) and slings, should facilitate efficient binding of the selectin ligands to the surface E-selectin and thus enable slow and stable rolling of the cell (Figure 7B).

In conclusion, our results suggest that during the initial step of HSPC migration, the selectin ligands are spatially confined to the tethers and slings through the development of the tethers from single microvilli and their motional freedom on the tethers and slings is enhanced by the detachment of the membrane from actin cytoskeleton during the formation of the tethers. These mechanisms enable the efficient utilization of the limited amount of the selectin ligands, which contributes to overcome the slow on rate of binding to the underlying E-selectin (AbuSamra et al., 2015; AbuSamra et al., 2017) to achieve effective selectin-ligand binding, resulting in this slow and stable cell rolling.

Acknowledgments

We thank Ms. Ohoud M. Alharbi for the SEM images of KG1a cells. The research reported in this publication was supported by funding from the King Abdullah University of Science and Technology (KAUST) and the KAUST Office of Sponsored Research under Award No. CRG R2 13 MERZ KAUST 1. We would like to thank Ms. Samar A. Rustum and Ms. Umm Habiba for their support in the management of the lab.

Author Contributions

S.H. and J.S.M conceived the project. B.A.A. designed the in vitro cell rolling assay and single-molecule fluorescence imaging experiments. K.A.Z. designed the super-resolution fluorescence microscopy experiments. A.R. prepared cells for SEM imaging? B.A.A. and A.R. conducted the fluorescence imaging experiments with the support of S.N. and analyzed the data with the support of M.F.S. K.A.Z. conducted the super-resolution fluorescence imaging experiments and analyzed the data. B.A.A. conducted the flow cytometry experiments with the support of F.A. M.A. prepared the CD34 knockdown KG1a cells. A.S.A. prepared the primary $CD34^{pos}$-HSPCs. M.A., A.S.A., A.R., and S.N. conducted and analyzed the fluorescence imaging experiments related to the CD34 knockdown KG1a cells and the primary human $CD34^{pos}$-HSPCs. J.S.M. provided the cell lines. S.H., J.S.M., and B.A.A. wrote the manuscript. All authors discussed the results.

Declaration of Interests

The authors declare no competing interests.

Figures and legends

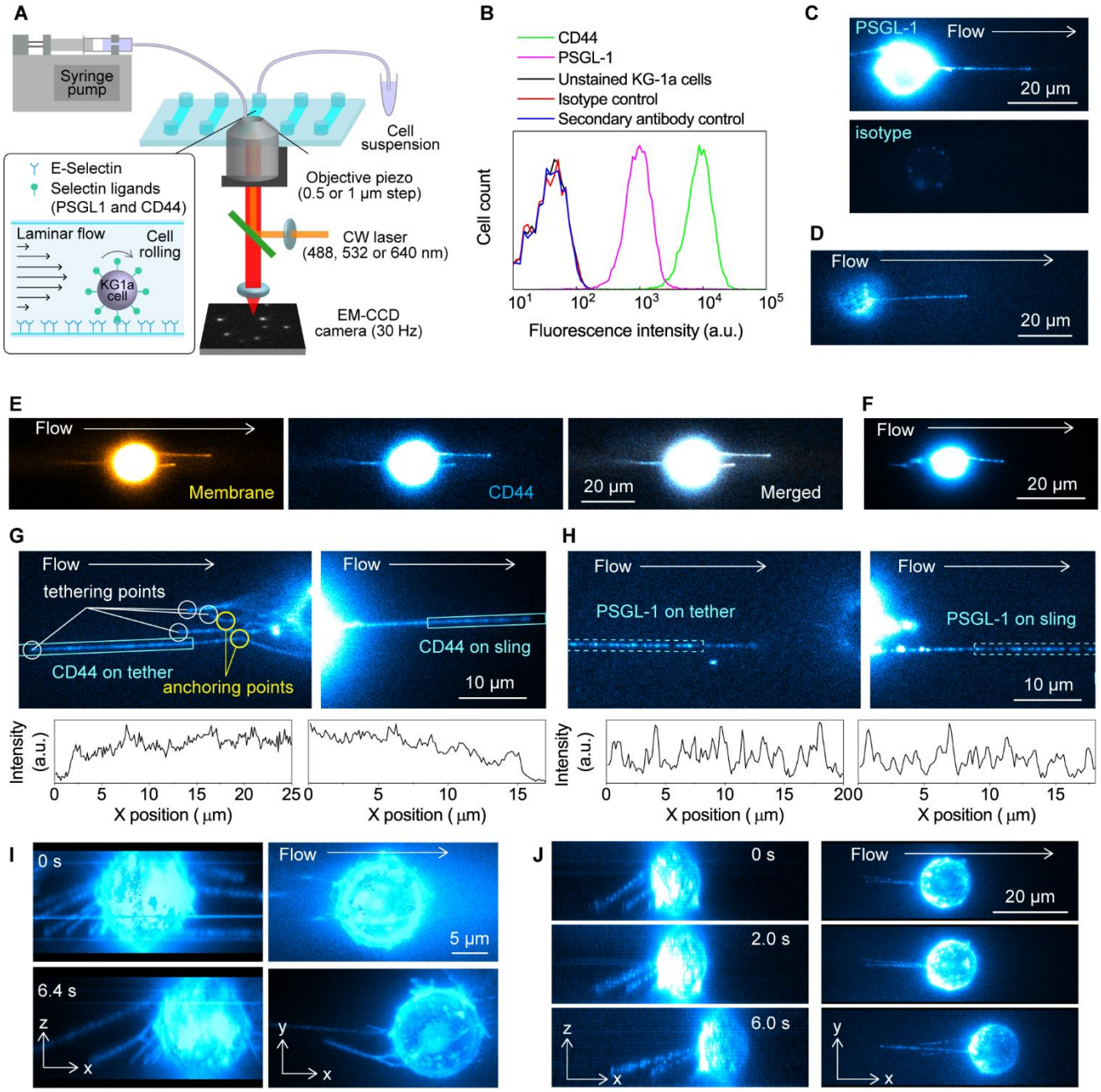

Figure 1. Single-molecule visualization of selectin ligands on the tethers and slings. (A) Schematic illustration describing the custom-built microfluidics-based single-molecule imaging setup. (B) Flow cytometric analysis of the binding specificity of CD44 and PSGL-1 antibodies. CD44 (green) and PSGL-1 (magenta) on KG1a cells were immunostained by antibodies against CD44 and PSGL-1 and Alexa-Fluor-488-conjugated secondary antibody against the isotype of the CD44 and PSGL-1 antibodies. Unstained KG1a cells (black), isotype control labeled cells (red), and secondary alone-labeled cells (blue) were included as controls. This is a representative experiment of n=2 independent experiments. (C) Binding specificity of the antibody

characterized by fluorescence imaging. (top) Fluorescence image of PSGL-1 molecules on a rolling KG1a cell over the surface-deposited E-selectin molecules that were immunostained by Alexa-Fluor-555-conjugated antibody. (bottom) Fluorescence image of an isotype control labeled KG1a cell that was injected into the fluidic chambers at conditions identical to those for the PSGL-1 immunostained cells. (D) Immunofluorescence image of PSGL-1 on a rolling KG1a cell over E-selectin captured using the Fab fragment of the anti-PSGL-1 antibody. The PSGL-1 molecules on the KG1a cells were immunostained by the Alexa-Fluor-555-conjugated Fab fragment of the anti-PSGL-1 antibody. (E) Two-color fluorescence images of the cell membrane (left, stained by Vybrant DiO dye) and CD44 (center, immunostained by Alexa-Fluor-647-conjugated anti-CD44 antibody) captured during the KG1a cell rolling over E-selectin. The right panel shows merged image. (F) Formation of the tethers and slings on primary human $CD34^{pos}$-HSPCs rolling over E-selectin. An example of the fluorescence images of CD44 (immunostained by Alexa-Fluor-647-conjugated anti-CD44 antibody) captured during human CD34pos-HSPC rolling over E-selectin. (G) Immunofluorescence image of the CD44 molecules on the tethers (top left) and slings (top right) formed during cell rolling over E-selectin. The bottom left and bottom right panels show fluorescence intensity profiles along the tethers and slings obtained from cyan regions in the top left and top right panels, respectively. (H) Immunofluorescence image of the PSGL-1 molecules (immunostained by Alexa-Fluor-555-conjugated anti-PSGL-1 antibody) on the tethers (top left) and slings (top right) formed during cell rolling over E-selectin. The bottom left and bottom right panels show fluorescence intensity profiles along the tethers and slings obtained from cyan regions in the top left and top right panels, respectively. (I) 3D views of the tethers and slings formed on a KG1a cell rolling over E-selectin by CD44. Side view (left) and top view (right) of the 3D reconstructed time-lapse fluorescence images of CD44 (immunostained by Alexa-Fluor-647-conjugated anti-CD44 antibody) captured during cell rolling over E-selectin. The 3D images were reconstructed by recording fluorescence images of the cell at 53 different Z-axis positions with 0.5 μm step size. The single 3D images were therefore captured every 1.6 sec (30 ms exposure time at each Z-position). (J) 3D views of the tethers formed on a KG1a cell rolling over E-selectin by PSGL-1. Side view (left) and top view (right) of the 3D reconstructed time-lapse fluorescence images of PSGL-1 (immunostained by Alexa-Fluor-555-conjugated anti-PSGL-1 antibody) captured during cell rolling over E-selectin. The 3D images were reconstructed by recording fluorescence images of the cell at 33 different Z-axis positions with 1.0 μm step size. The single 3D images were therefore captured every 1.0 sec (30 ms exposure time at each Z-position). All the fluorescence images of the rolling cells were captured by injecting KG1a cells into the microfluidic chambers at a shear stress of 2 dyne cm^{-2} whose surface was coated by the rh E-selectin at a density of 15 molecules μm^{-2}.

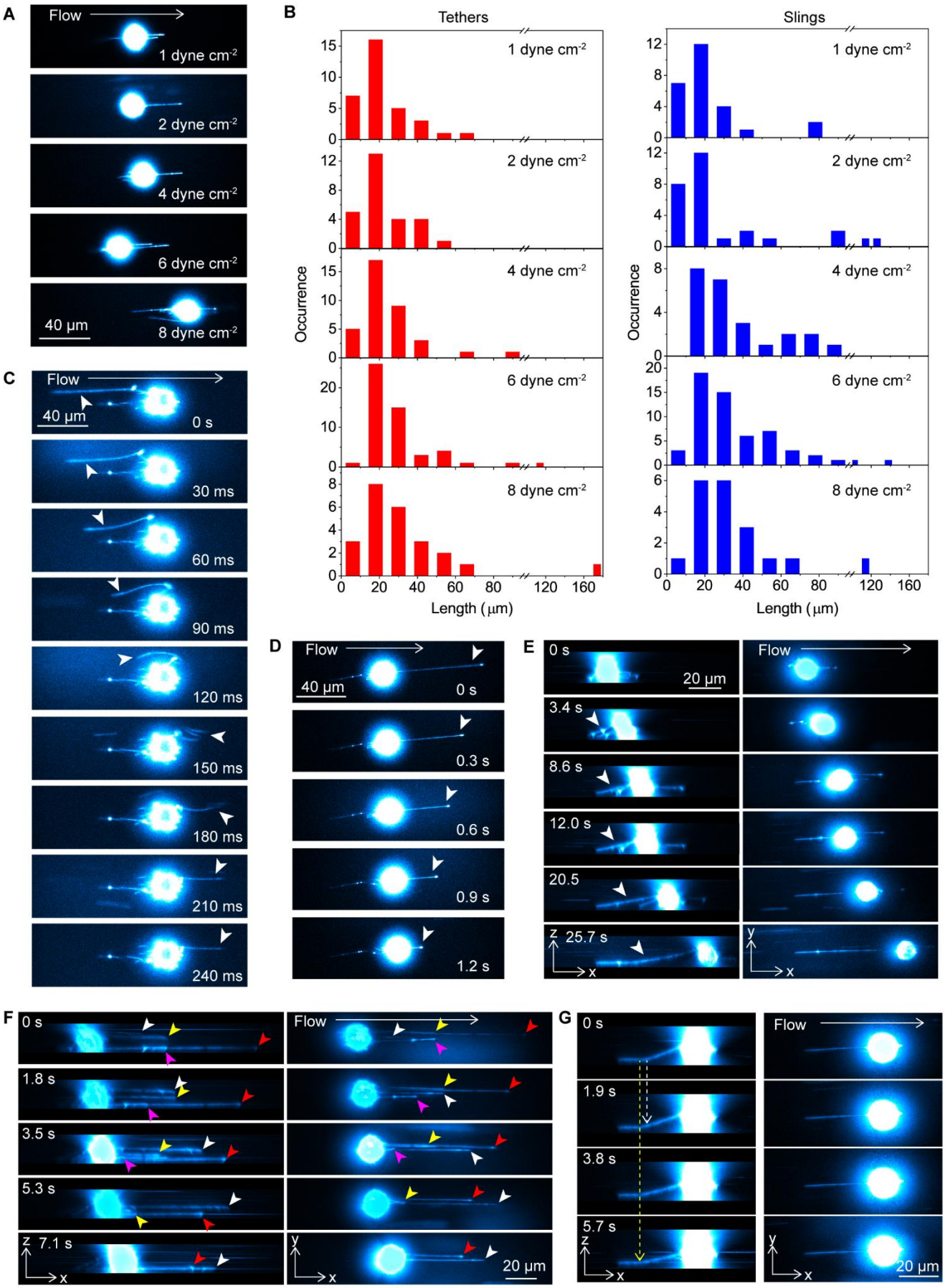
A
Flow
1 dyne cm-2
2 dyne cm-2
4 dyne cm-2
6 dyne cm-2
8 dyne cm-2
40 μm
B
Tethers
Slings
Occurrence
Length (μm)
C
0 s
30 ms
60 ms
90 ms
120 ms
150 ms
180 ms
210 ms
240 ms
D
0.3 s
0.6 s
0.9 s
1.2 s
E
20 μm
3.4 s
8.6 s
12.0 s
20.5
25.7 s
F
1.8 s
3.5 s
5.3 s
7.1 s
G
1.9 s
3.8 s
5.7 s

Figure 2. Spatiotemporal dynamics of the tethers and slings during cell rolling. (A) Shear force-dependent formation of the tethers and slings on KG1a cells rolling over E-selectin. Fluorescence images of CD44 (immunostained by Alexa-Fluor-647-conjugated anti-CD44 antibody) captured during cell rolling over the surface-deposited E-selectin molecules. The cells were injected into the chambers at a shear stress of 1, 2, 4 or 8 dyne cm^{-2}. (B) Length of the tethers and slings formed on KG1a cells rolling over E-selectin. Frequency histograms of the length of tethers (red bars) and slings (blue bars) formed during the KG1a cells rolling over E-selectin. (C) Conversion of tethers into slings observed for KG1a cells rolling over E-selectin. Time-lapse fluorescence images of CD44 (immunostained by Alexa-Fluor-647-conjugated anti-CD44 antibody) captured during cell rolling over E-selectin. The arrow heads show a tether that is converted into a sling upon the detachment of the tethering point from the E-selectin surface. The cells were injected into the chambers at a shear stress of 6 dyne cm^{-2}. (D) Retraction of the slings. Time-lapse fluorescence images of CD44 (immunostained by Alexa-Fluor-647-conjugated anti-CD44 antibody) captured during cell rolling over E-selectin. The arrow heads show the slings with this retraction behavior. The cells were injected into the chambers at a shear stress of 8 dyne cm^{-2}. (E) 3D views of the elongation of the tether formed on a KG1a cell rolling over E-selectin. Side view (left) and top view (right) of the 3D reconstructed time-lapse fluorescence images of CD44 (immunostained by Alexa-Fluor-488-conjugated anti-CD44 antibody) captured during cell rolling over E-selectin. The 3D images were reconstructed by recording fluorescence images of the cell at 57 different Z-axis positions with 0.5 μm step size. The single 3D images were therefore captured every 1.7 sec (30 ms exposure time at each Z-position). The arrowheads indicate the tether that shows elongation behavior. The cells were injected into the chambers at a shear stress of 2 dyne cm^{-2}. (F) 3D views of the slings formed on a KG1a cell that show changes in the Z-axis positions during cell rolling over E-selectin. Side view (left) and top view (right) of the 3D reconstructed time-lapse fluorescence images of CD44 (immunostained by Alexa-Fluor-488-conjugated anti-CD44 antibody) captured during cell rolling over E-selectin. The 3D images were reconstructed by recording fluorescence images of the cell at 59 different Z-axis positions with 0.5 μm step size. The single 3D images were therefore captured every 1.8 sec (30 ms exposure time at each Z-position). The arrow heads in white, yellow, red and magenta show four different slings formed during cell rolling. The cells were injected into the chambers at a shear stress of 2 dyne cm^{-2}. (G) 3D views of the tether formed on a KG1a cell that show changes in the position of the anchoring points during cell rolling over E-selectin. Side view (left) and top view (right) of the 3D reconstructed time-lapse fluorescence images of CD44 (immunostained by Alexa-Fluor-488-conjugated anti-CD44 antibody) captured during cell rolling over E-selectin. The 3D images were reconstructed by recording fluorescence images of the cell at 63 different Z-axis positions with 0.5 μm step size. The single 3D images were therefore captured every 1.9 sec (30 ms exposure time at each Z-position). The white and yellow arrows show the positions of the two anchoring points formed on the tether. The first anchoring point (white arrow) is detached during cell rolling, whereas the second anchoring point (yellow arrow) continues attaching to the surface E-selectin. The cells were injected into the chambers at a shear stress of 2 dyne cm^{-2}. All the fluorescence images of the rolling cells were captured by injecting KG1a cells into the microfluidic chambers whose surface was coated by the rh E-selectin at a density of 15 molecules μm^{-2}.

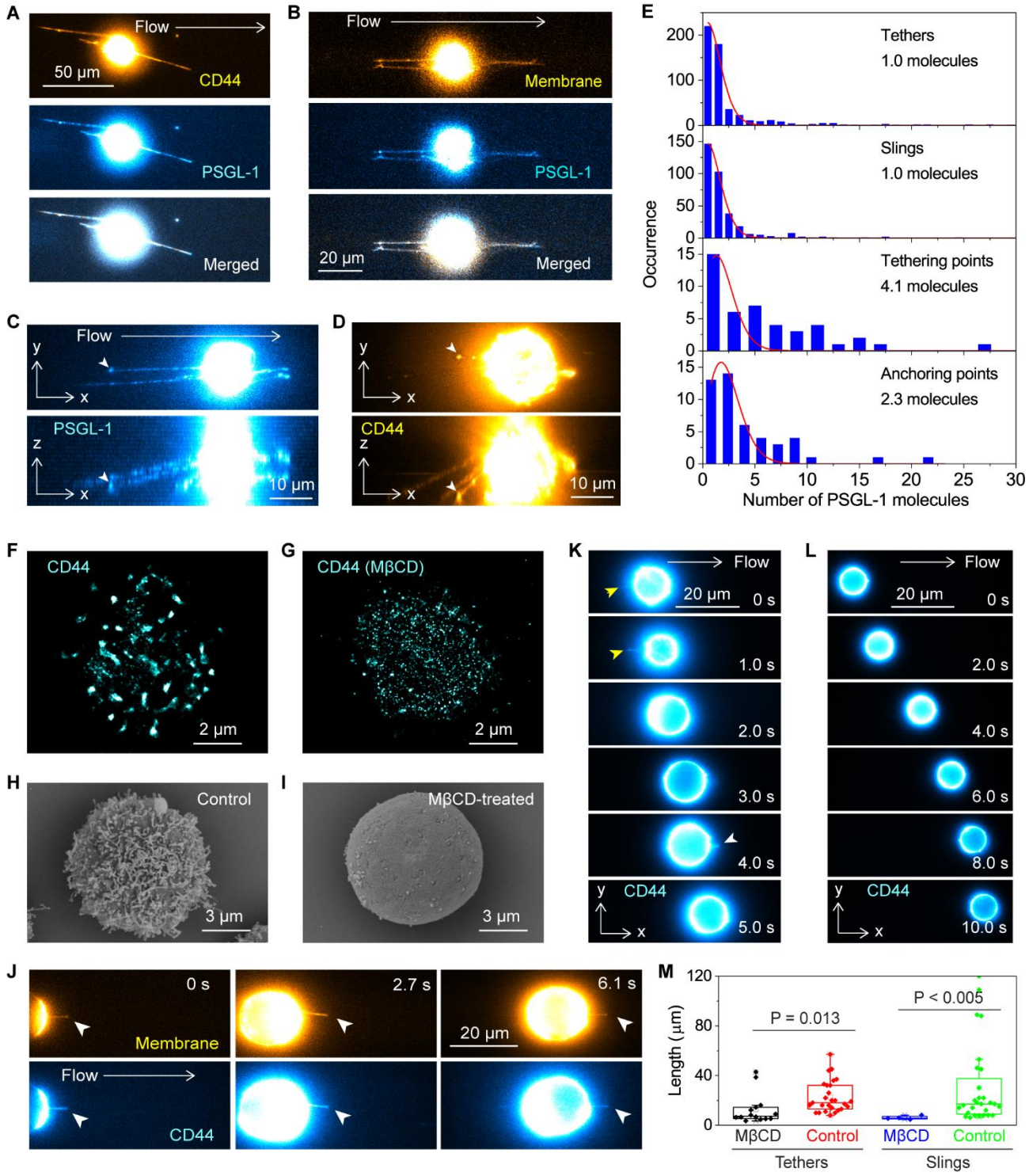

Figure 3. Spatial clustering of the selectin ligands on microvilli enables efficient formation of tethers and slings. (A) Colocalization of CD44 and PSGL-1 on the tethers and slings formed on a KG1a cell rolling over E-selectin. Two-color fluorescence image of CD44 (top, yellow, immunostained by Alexa-Fluor-647-conjugated anti-CD44 antibody) and PSGL-1 (middle, cyan, immunostained by Alexa-Fluor-488-conjugated anti-PSGL-1 antibody) captured during cell

rolling over E-selectin. The merged image is displayed in the bottom panel. (B) Colocalization of cell membrane and PSGL-1 on the tethers and slings formed on a KG1a cell rolling over E-selectin. Two-color fluorescence images of the cell membrane (top, yellow, stained by Vybrant DiO dye) and PSGL-1 (middle, cyan, immunostained by Alexa-Fluor-647-conjugated anti-PSGL-1 antibody,) captured during cell rolling over the surface-deposited E-selectin molecules. The merged image is displayed in the bottom panel. (C) Top view (top) and side view (bottom) of the 3D reconstructed fluorescence images of the PSGL-1 molecules (left, immunostained by Alexa-Fluor-555-conjugated anti-PSGL-1 antibody) captured during the KG1a cells rolling over E-selectin. The 3D images were reconstructed by recording fluorescence images of the cell at 40 different Z-axis positions with 1 μm step size. (D) Top view (top) and side view (bottom) of the 3D reconstructed fluorescence images of the CD44 molecules (immunostained by Alexa-Fluor-647-conjugated anti-CD44 antibody) captured during the KG1a cells rolling over E-selectin. The 3D images were reconstructed by recording fluorescence images of the cell at 59 different Z-axis positions with 0.5 μm step size. (E) Frequency histograms of the number of the PSGL-1 molecules in each spot on the tethers and slings and at the tethering points and anchoring points of the KG1a cells. The solid lines show Poissonian fittings. (F) Super-resolution fluorescence localization microscopy image of CD44 (immunostained by anti-CD44 515 antibody followed by Alexa-Fluor-647-conjugated secondary antibodies) on the KG1a cell. (G) Super-resolution fluorescence localization microscopy image of CD44 (immunostained by anti-CD44 515 antibody followed by Alexa-Fluor-647-conjugated secondary antibodies) on the methyl-β-cyclodextrin (MβCD)-treated KG1a cell. (H) Scanning electron microscopy image of the KG1a cell. (I) Scanning electron microscopy images of the MβCD-treated KG1a cell. (J) Spatial colocalization of CD44 and membrane tethers/slings on the MβCD-treated KG1a cells. Time-lapse two-color fluorescence images of the cell membrane (top, stained by Vybrant DiO dye) and CD44 (bottom, immunostained by Alexa-Fluor-647-conjugated anti-CD44 antibody) captured during the MβCD-treated KG1a cell rolling over E-selectin. White arrowheads show slings formed during the cell rolling. (K) Time-lapse fluorescence images of the CD44 molecules (immunostained by Alexa-Fluor-647-conjugated anti-CD44 antibody) captured during the MβCD-treated KG1a cell rolling over E-selectin. The yellow and white arrowheads highlight tether and sling, respectively. (L) Time-lapse fluorescence images of the CD44 molecules (immunostained by Alexa-Fluor-647-conjugated anti-CD44 antibody) captured during CD34 knockdown (CD34-KD) KG1a cell rolling over E-selectin. (M) Box plots showing the length of individual tethers and slings on the control and MβCD-treated KG1a cells. All the fluorescence images of the rolling cells were captured by injecting KG1a cells into the microfluidic chambers at a shear stress of 2 dyne cm^{-2} whose surface was coated by the rh E-selectin at a density of 15 molecules μm^{-2}.

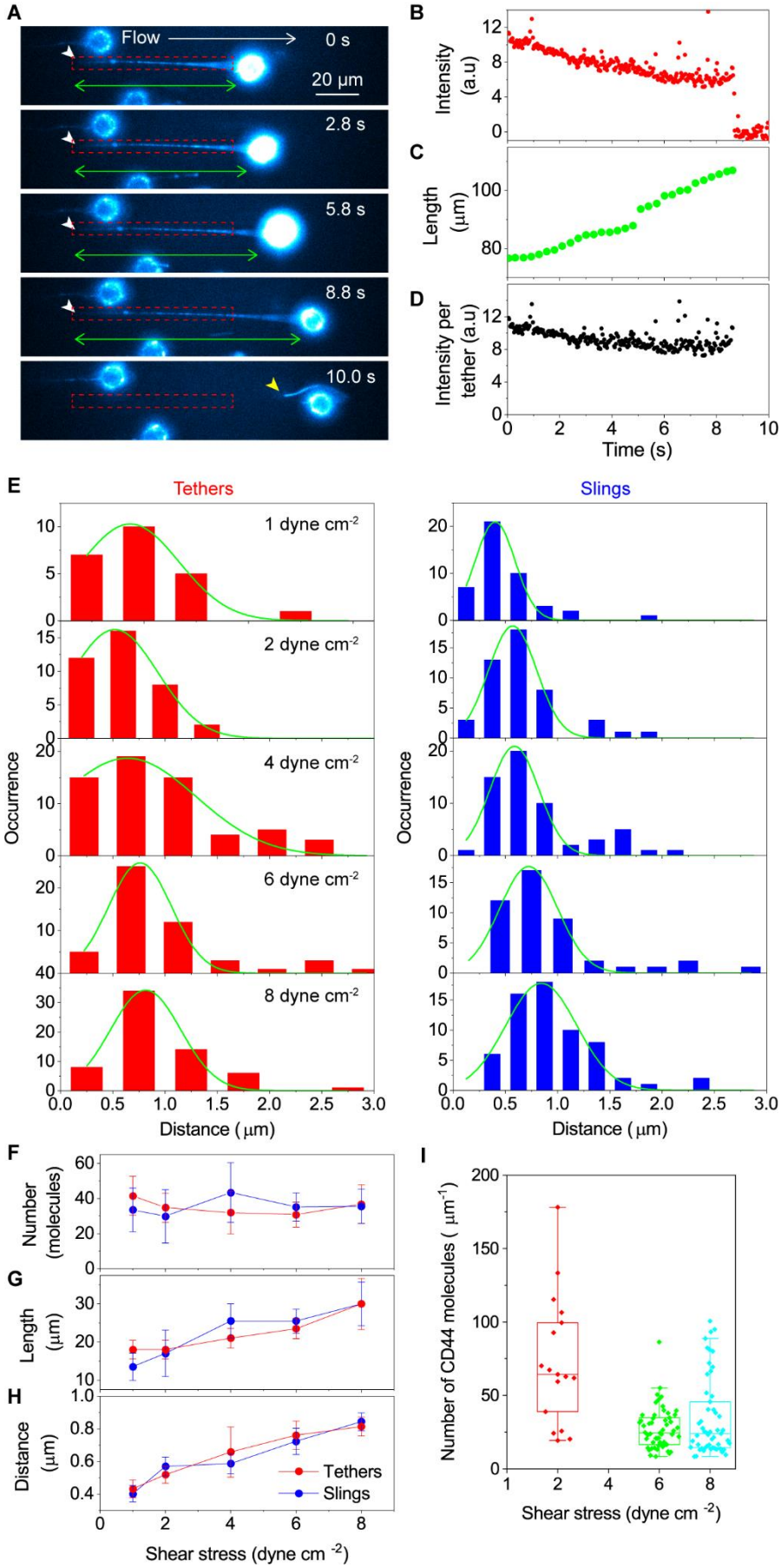
A
Flow
0 s
20 μm
2.8 s
5.8 s
8.8 s
10.0 s
B
Intensity (a.u)
C
Length (μm)
D
Intensity per tether (a.u)
Time (s)
E
Tethers
Slings
1 dyne cm-2
2 dyne cm-2
4 dyne cm-2
6 dyne cm-2
8 dyne cm-2
Occurrence
Distance (μm)
F
Number (molecules)
G
Length (μm)
H
Distance (μm)
Tethers
Slings
Shear stress (dyne cm -2)
I
Number of CD44 molecules (μm-1)
Shear stress (dyne cm -2)

Figure 4. Spatial confinement of the selectin ligands to the tethers and slings. (A) Time-lapse fluorescence images of the PSGL-1 molecules (immunostained by Alexa-Fluor-555-conjugated anti-PSGL-1 antibody) on the KG1a cell captured during cell rolling over E-selectin (15 molecules μm^{-2}) at a shear stress of 2 dyne cm^{-2}, which shows the elongation of the tether. The white arrowheads show the tethering point. The yellow arrowhead show the tether detached from the surface E-selectin. (B) Time-lapse integrated fluorescence intensities of the PSGL-1 molecules obtained from the region designated by the red dashed boxes in (A). (C) Time-dependent change in the length of the tether obtained from the time-lapse fluorescence images of PSGL-1 displayed in (A) green arrows. (D) Time-dependent change in the integrated fluorescence intensity of the PSGL-1 molecules obtained from the whole tether formed during cell rolling displayed in (A). (E) Distance between the PSGL-1 spots on the tethers and slings formed on KG1a cells rolling over E-selectin. Frequency histograms of the distance between the adjacent fluorescent spots of PSGL-1 on the tethers (red bars) and slings (blue bars) formed during the KG1a cells rolling over E-selectin. (F) Shear stress dependence of the mean numbers of the PSGL-1 molecules per tether and sling. (G) Shear stress dependence of the mean lengths of the tether and sling. (H) Shear stress dependence of the mean distances between adjacent PSGL-1 molecules on the tether and sling. The error bars show the standard deviations determined by 19 – 58 data. (I) Number of CD44 molecules per unit length of slings. The CD44 molecules on the KG1a cells were immunostained by the Alexa-Fluor-647-conjugated anti-CD44 antibody. The fluorescence images were recorded during KG1a cell rolling over E-selectin (15 molecules μm^{-2}) at shear stresses of 1, 2, 4, 6 and 8 dynes cm^{-2}.

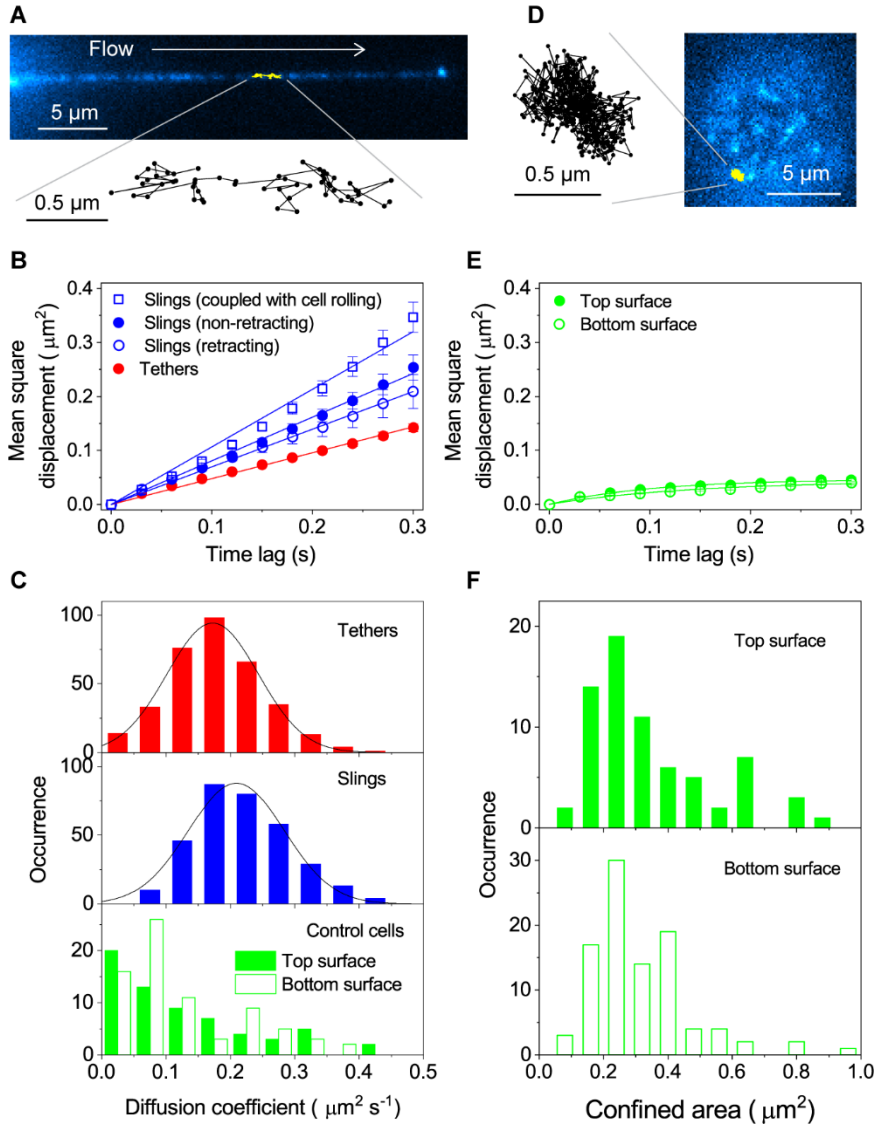

Figure 5. Single-molecule tracking analysis of PSGL-1 on the tethers and slings. (A) Single-molecule fluorescence images of PSGL-1 (immunostained by Alexa-Fluor-555-conjugated anti-PSGL-1 antibody) on the sling of the KG1a cell formed during cell rolling over E-selectin (15 molecules μm^{-2}) at a shear stress of 2 dyne cm^{-2}. An example of the single-molecule diffusion trajectories obtained from the time-lapse fluorescence images is shown by the yellow line. (B) Mean square displacement (MSD) versus time lag plots obtained for the PSGL-1 molecules diffusing on the tethers (red), stable slings without the effect of the cell rolling (open blue circle), retracting slings without the effect of the cell rolling (blue circle), and stable slings with the effect of the cell rolling (open blue square). The error bars show the standard errors of the mean determined by 340, 47, 169 and 104 MSD plots obtained for the PSGL-1 molecules diffusing on the tethers, retracting slings, non-retracting slings and stable slings with the effect of the cell rolling, respectively. (C) Frequency histograms of the diffusion coefficient of the PSGL-1 molecules on the tethers (top) and slings (middle) of the KG1a cells formed during cell rolling over E-selectin (15 molecules μm^{-2}) at a shear stress of 2 dyne cm^{-2}. The bottom panel shows a

frequency histogram of the diffusion coefficient of the PSGL-1 molecules on the microvilli of the control KG1a cells at the top (green bars) and bottom (open green bars) surface of the cells. The diffusion coefficients were calculated by fitting the MSD plots obtained from the individual diffusion trajectories to Eq. 4 and Eq. 5 for the molecules on the tethers and slings and the molecules localized to the microvilli, respectively. The solid lines show Gaussian fittings. (D) Single-molecule fluorescence images of PSGL-1 (immunostained by Alexa-Fluor-488-conjugated anti-PSGL-1 antibody) on the microvilli of the control KG1a cell. An example of the single-molecule diffusion trajectories obtained from the time-lapse fluorescence images is shown in the yellow line. (E) MSD versus time lag plots obtained for the PSGL-1 molecules localized on the microvilli of the KG1a cells at the top (green circle) and bottom (open green circle) surface of the cells. The error bars show the standard errors of the mean determined by 126 and 129 MSD plots obtained for the PSGL-1 molecules localized on the microvilli of the control KG1a cells at the top and bottom surface of the cells. (F) Frequency histograms of the confine area of the diffusing PSGL-1 molecules on the microvilli of the control KG1a cells at the top (top, green bars) and bottom (bottom, open green bars) surface of the cells. The confined areas were calculated by fitting the MSD plots obtained from the individual diffusion trajectories to Eq. 5. All the fluorescence images of the rolling cells were captured by injecting KG1a cells into the microfluidic chambers at a shear stress of 2 dyne cm^{-2} whose surface was coated by the rh E-selectin at a density of 15 molecules μm^{-2}.

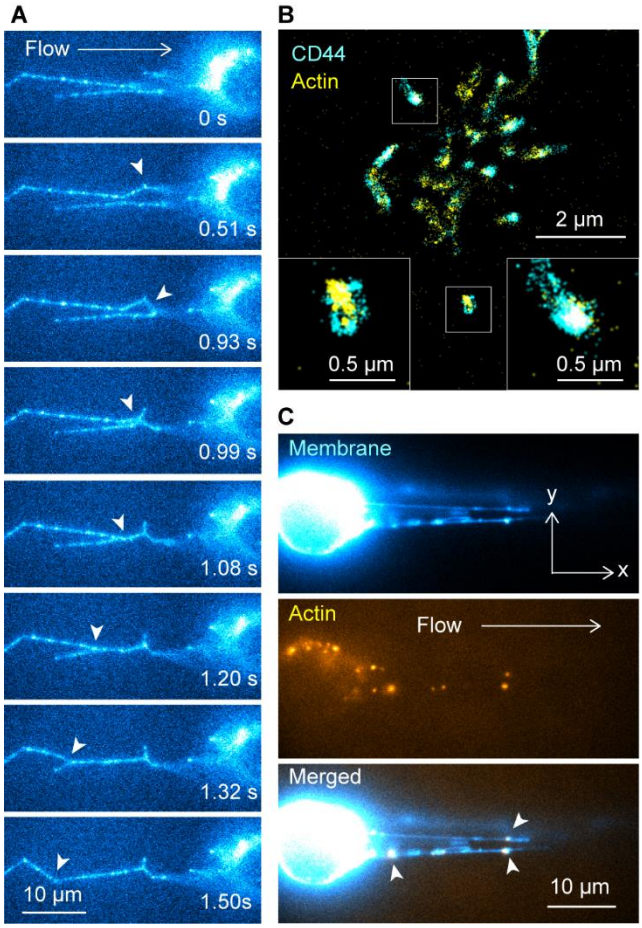

Figure 6. Detachment of cell membrane from actin cytoskeleton during the tether formation. (A) Time-lapse fluorescence images of the PSGL-1 molecule (immunostained by Alexa-Fluor-555-conjugated anti-PSGL-1 antibody) on the KG1a cell captured during cell rolling over E-selectin, which show the merger of the multiple tethers. The white arrowheads show the regions in which the merger of the tethers occurs. (B) Two-color super-resolution fluorescence localization microscopy image of CD44 (cyan, immunostained by anti-CD44 515 antibody followed by Alexa-Fluor-647-conjugated secondary antibodies) and actin (yellow, labeled by Alexa-Fluor-488-conjugated phalloidin) on the control KG1a cell. The insets show enlarged views of the yellow regions. (C) Two-color fluorescence images of the cell membrane (cyan, stained by Vybrant DiO dye) and actin (yellow, labeled by silicon-rhodamine-conjugated jasplakinolide) on the slings of the KG1a cells formed during cell rolling over E-selectin. The white arrowheads show the regions in which the patches of actin colocalize with the slings. All the fluorescence images of the rolling cells were captured by injecting KG1a cells into the microfluidic chambers at a shear stress of 2 dyne cm^{-2} whose surface was coated by the rh E-selectin at a density of 15 molecules μm^{-2}.

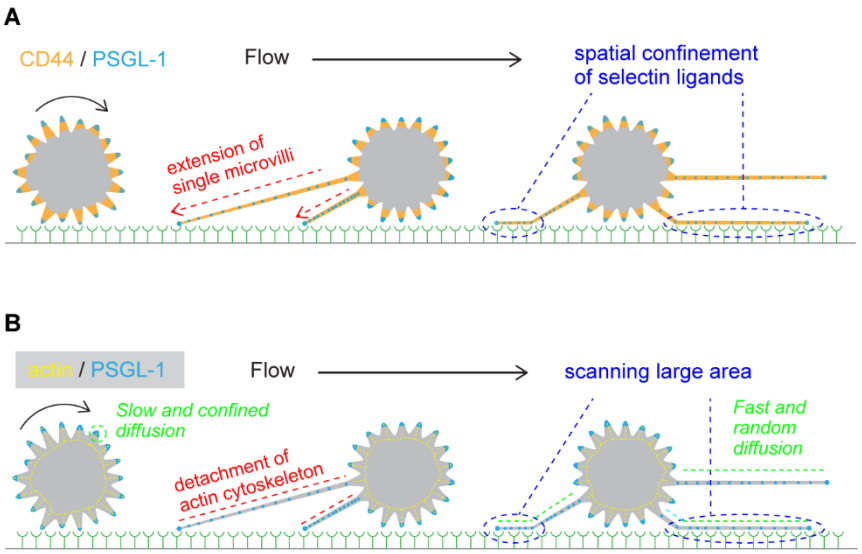

Figure 7. Fast and random diffusional motion of selectin ligands spatially confined to the membrane tethers and slings promote stable cell rolling. (A) Schematic illustration describing how the spatial confinement of the selectin ligands into the tethers and slings due to the formation of individual tethers from single microvilli promote stable and slow rolling of the cell on E-selectin. (B) Schematic illustration describing how the faster and random diffusional motion of the selectin ligands on the tethers and slings, due to the detachment of the cell membrane from the cortical actin cytoskeleton during the tether formation, promote stable and slow rolling the cell on E-selectin.

Methods

Cell culturing and treatments. Human acute myelogenous leukemia cell lines, KG1a cells (ATCC CCL-246.1) were maintained in the lab using cell culturing facility in RPMI 1640 (1×) media (Gibco) that contains 10 % fetal bovine serum (Corning) and antimicrobial agents (100 U ml^{-1} penicillin, 100 μg ml^{-1} streptomycin, Hyclone) incubated at 37° C in presence of controlled 5% CO_2. For the disruption of lipid raft microdomains, the KG1a cells were treated with methyl-β-cyclodextrin (MβCD). Briefly, 10^6 ml^{-1} KG1a cells were washed three times by HBSS buffer (pH = 7.0 – 7.4) and incubated in serum-free Iscove's modified Dulbecco's medium (IMDM, Gibco) with 10 mM HEPES buffer (Sigma) and 10 mM MβCD (Sigma) at 37° C for 30 min. The viability of the cells after the treatment was confirmed by trypan blue staining. For siRNA knockdown of CD34 in KG1a cells, KG1a cells were first collected and treated for 20 min at 37°C with bromelain (250 ug/ml; Sigma) in RPMI media with 10% FBS. Cells were then washed twice with PBS and prepared for transfection. The bromelain treated KG1a cells were then transfected using 250 pmol of CD34 siRNA (Silencer Select, Life technologies; 4392420-s2644) or 250 pmol of a scrambled control siRNA (Silencer Select, Life technologies; 4390843). Transfection was done using the SE Cell Line 4D-Nucleofector™ X Kit (Lonza). The company protocol was followed to achieve the knockdown. Cells were then collected after 48 h and prepared for Western blot analysis to determine the extent of the CD34 inhibition.

Preparation of human $CD34^{pos}$ HSPCs. Primary human $CD34^{pos}$ HSPCs isolated from umbilical cord blood ($CD34^{pos}$HSPCs) and the mononuclear cells (MNC) from whole cord blood were purchased from ALL Cells (USA). For $CD34^{pos}$HSPCs isolation from whole cord blood, the MNCs were washed and filtered through a 100 μm cell strainer (BD Falcon) followed by

lineage depleton by negative selection using a lineage cell depletion cocktail (Milteny Biotec). The lineage depleted fraction was stained with 13 markers for lineage-specfic monoclonal antibodies FITC (CD2, CD3, CD4, CD11b, CD14, CD15, CD24, CD10, CD41, CD20, CD66c, CD127, CD33) (Biolegend and BD) and Pacific blue conjugated anti-CD34 (Biolegend), for 30 min at 4°C. Before sorting, 7-AAD was added to the tubes. Afterwards, 13Lin−CD34^{pos} cells were collected by the fuorescence- activated cell sorter (FACSAria, BD Biosciences, San Jose, CA, USA).

For CD34^{pos} HSPCs, the cells were thawed using stem span SFEM II medium (Stem Cell Technologies, Canada) and washed 1x with the same medium. The cells were resuspended in 1 mL of medium contained 1x Stem Span Cytokine Cocktail CC100 (Stem Cell Technologies, Canada) in 24-well plate, then the cells were analyzed within 24 hours.

Preparation and functionalization of the microfluidic chambers. Commercially available microfluidic chambers, μ-slide VI 0.1 uncoated (ibidi GmbH) were used for *in vitro* cell rolling assay. Recombinant homodimeric human (rh) E-selectins (Sino Biological) were deposited on the inner surface of the microfluidic chambers by incubating with 20 μl of the rh E-selectin (0.5 – 4 μg ml^{-1}) at 4° C for overnight. After the incubation, the chambers were washed 3 times using 1× Hank's balanced Salt Solution (HBSS, Gibco) and blocked with 1% Bovine Serum Albumin (BSA, Sigma Aldrich) by incubating the chambers at 4° C for 1-2 hours. The chambers were then washed by 1× HBSS three times.

Estimation of the surface density of the rh E-selectin. A monoclonal anti-human E-selectin antibody (HCD62E clone, Biolegend) was labeled with Alexa-Fluor-647 dye as described below. The Alexa-Fluor-647-conjugated anti-E-selectin was diluted into HBSS at the concentration of

10 μg ml^{-1}. 20 μl of the Alexa-Fluor-647-conjugated anti-E-Selectin antibody was introduced into the microfluidic chambers on which the homodimeric rh E-Selectin was deposited. The chambers were incubated with the antibody at 4° C for 1 hour. The fluorescence from the Alexa-Fluor-647-conjugated anti- E-Selectin antibody bound to the surface rh E-selectin was recorded using a custom-built single-molecule fluorescence imaging setup (see below). The surface density of the rh E-selectin was calculated by comparing the integrated fluorescence intensity obtained from a unit area (1 μm^2) of the rh E-selectin-deposited surface with the intensity obtained from single rh E-Selectin molecules labeled by the Alexa-Fluor-647-conjugated anti-E-Selectin antibody. The fluorescence intensity from single rh E-Selectin molecules labeled by the antibodies was determined by depositing the Alexa-Fluor-647-conjugated anti-E-Selectin antibody on the rh E-selectin-deposited surface at very low concentration (0.02 μg ml^{-1}) and measuring the fluorescence intensities of the individual fluorescent spots obtained from the single rh E-selectin molecules labeled by the antibodies.

Cell rolling assay using bright-filed microscope. The rh E-selectin-deposited microfluidic chambers were connected to a syringe pump (Harvard Apparatus, PHD Ultra) using a silicone tubing (inner diameter of 0.8 mm, ibidi GmbH) and mounted on an inverted optical microscope (Olympus, CKX41). KG1a cells were suspended in HBSS buffer containing 0.7 mM of Ca^{2+} (anhydrous $CaCl_2$, Sigma Aldrich) and 1 % (w/v) BSA. The rolling behavior of the cells in this perfusion buffer was observed using the inverted light microscope that is equipped with a 20× objective lens (Olympus, LCAch N 20X PHP) and XC10 CCD camera (Olympus). The transmitted images were recorded by the CCD camera using CellSens imaging software provided by Olympus. All images were recorded at the frame rate of 15 fps with 30 ms exposure time. The pixel size of the CCD camera is 6.45 μm. The KG1a cells were perfused into the microfluidic

chamber mounted on the microscope stage at the flow rate of 100 dyne cm^{-2}, then the flow rate was decreased gradually to reach a constant shear stress of 4 dyne cm^{-2}, 2 dyne cm^{-2}, 1 dyne cm^{-2}, 0.5 dyne cm^{-2}, or 0.25 dyne cm^{-2} where cell rolling behavior was monitored for 78 seconds in each experiment. The rolling velocities were calculated using CellSens or TrackMate, an Image J plugin. The rolling velocities were estimated by measuring the distance travelled by each cell after being bound to the immobilized rh E-selectins. The number of the bound cells was determined by counting the number of the attached cells in a field of view (0.444 mm × 0.335 mm size).

Fluorescence labeling of the antibodies. The fluorescence labeling of the antibodies by Alexa-Fluor-488 dye (Invitrogen), Alexa-Fluor-555 dye (Invitrogen), and Alexa-Fluor-647 dye (Invitrogen) was conducted by following the manufacturer's instructions. The labeled antibodies were mouse anti-human E-selectin (HCD62E clone), mouse anti-human CD44 (515 clone, Ms IgG1, κ, BD Bioscience) and mouse anti-human PSGL-1 (KPL-1 clone, Ms IgG1, κ, BD Bioscience) and mouse anti-human CD34 (QBEND 10 clone, Ms IgG1, Bio-Rad). Briefly, the Alexa-Fluor dyes conjugated to N-hydroxysuccinimide (NHS) were dissolved in dimethylsulfoxide (DMSO, Sigma-Aldrich, 276855) to a final concentration of 10 mg ml^{-1}. The antibodies were dissolved in 0.1 M sodium bicarbonate (pH = 8.3 – 8.4) at a concentration of 6.5 mg ml^{-1}. 30.7 µl of the antibody solution and 2 µl Alexa-Fluor dye solution (i.e. mixing ratio of ten to one, which corresponds to the dye to antibody molar ratio of approximately 120 to 1) were mixed and incubated for 1 hour at room temperature. After the labeling reaction, 467 µl of HBSS was added to the reaction mixture. Free dyes in the mixture were removed by using a spin filter (Pall Corporation, Nanosep centrifugal devices with Omega membrane, OD010C34) at a centrifuge speed of 10,000 xg for 5 min. The solution was resuspended in HBSS and the

centrifugation was repeated several times. The final concentration of the antibodies and the labeling degree were determined by UV-vis absorption spectra of the Alexa-Fluor dye-conjugated antibodies. The degree of labeling was in the range of 4 – 9 dyes per antibody.

Fragmentation and fluorescence labeling of the antibodies. For the digestion and purification of the anti-PSGL-1 antibody (KPL-1 clone, IgG1), we used Pierce Mouse IgG1 Fab and F(ab´)2 Preparation Kit or Pierce Mouse IgG1 Fab and F(ab´)2 Micro Preparation Kit (Thermo Scientific). The kit uses immobilized ficin protease to efficiently digest mouse IgG1 into Fab or F(ab')2 fragments, depending on the concentration of cysteine and solution pH. Briefly, the digestion buffer was prepared by dissolving 43.9 mg of cysteine•HCl in 10 ml of the supplied Mouse IgG1 digestion buffer (pH = 5.6) to produce Fab fragments. Then, the immobilized enzyme was dispensed into the spin column, centrifuged and washed using the prepared digestion buffer. The antibody (1 mg ml^{-1}, 125 µl) was desalted using the accompanied Zeba column. The flow through of at least 100 µl that contained the antibody was incubated with the immobilized enzyme for 3-5 hours at 37 ^{o}C on an end-over-end mixer, which digested the antibody into Fab fragments. After the incubation, the column was put into a 2 ml collection tube and centrifuged at 5000 × g for 1 min to collect the digested antibodies. The collected flow through was incubated with protein A column for 10 min at room temperature on an end-over-end mixer, followed by centrifugation at 1000 × g for 1 min to separate the Fab fragments from Fc and undigested antibodies. The flow through that contained Fab fragments was collected. After the fragmentation and purification, concentrations of the anti-PSGL-1 antibody (KPL-1 clone, IgG1) and its fragments were determined by measuring the absorbance at 280 nm using UV-vis spectrophotometer (Thermo Scientific, NanoDrop 2000).

Fluorescence labeling of the Fab fragment of the anti-PSGL-1 antibody by the Alexa-Fluor dyes conjugated to N-hydroxysuccinimide (NHS) was conducted in a manner similar to the labeling of the whole antibody. The Fab fragment and the dye were mixed at the mixing ratio of thirty to one, which corresponds to the dye to antibody molar ratio of approximately 120 to 1. The degree of labeling with this mixing ratio was in the range of 1 – 3 dyes per Fab fragment.

Fluorescence labeling of the primary cells and KG1a cells. Prior to immunostaining of the KG1a and primary cells, the cells were incubated with Fc blocker (0.15 – 0.3 ml for each 1 x 10^6 cells, Innovex biosciences) on ice for 45 minutes, then washed three times with 1x HBSS. The cells were immunostained by either Alexa-Fluor-488-conjugated anti-PSGL-1, Alexa-Fluor-555-conjugated anti-PSGL-1, Alexa-Fluor-647-conjugated anti-PSGL-1, Alexa-Fluor-488-conjugated anti-CD44, or Alexa-Fluor-647-conjugated anti-CD44 for 45 min on ice at a concentration of 5 μg for each 10^6 cells. The immunostained cells were suspended in a Fluorobrite (Gibco) perfusion buffer containing 0.7 mM of Ca^{2+} at the density of 0.5 – 1 × 10^6 cells ml^{-1}. Then, the cells were injected into the rh E-selectin-deposited microfluidic chambers using the silicone tubing connected to the syringe pump. The KG1a or primary cells were perfused into the microfluidic chamber mounted on the stage of an inverted fluorescence microscope (Olympus, IX71) at the flow rate of 100 dyne cm^{-2}. Then the flow rate was decreased gradually to reach a constant shear stress of 1 – 8 dyne cm^{-2} where real-time fluorescence images of CD44 or PSGL-1 on the live KG1a or primary cells were recorded by using EMCCD camera connected to the iQ3 software (see below).

Two-color fluorescence imaging of CD44 and PSGL-1 on the KG1a cells were conducted by immunostaining both CD44 and PSGL-1 with a combination of either Alexa-Fluor-488-

conjugated anti-CD44 and Alexa-Fluor-647-conjugated anti PSGL-1 or Alexa-Fluor-647-conjugated anti-CD44 and Alexa-Fluor-488-conjugated anti PSGL-1. For the two color immunostaining, the KG1a cells were incubated simultaneously with the two antibodies (5 µg of each antibody for 10^6 cells) on ice for 45 min.

Two-color fluorescence imaging of CD44 and CD34 on KG1a and CD34 knockdown cells were conducted by immunostaining both CD44 and CD34 with a combination of Alexa-Fluor-647-conjugated anti CD44 and Alexa-Fluor-488-conjugated anti-CD34. For the two color immunostaining, KG1a cells were first incubated with CD44 antibody and then with CD34 antibody (5 µg of each antibody for 10^6 cells). Each incubation was done on ice cooled condition for 45 min.

We used Vybrant DiO (Molecular Probe) for staining plasma membrane of KG1a cells. The harvested and counted KG-1a cells were washed three times with serum free 1x IMDM. The staining solution was prepared by adding 1 µl of the Vybrant DiO stain to each 1 ml serum free IMDM. The 10^6 cells after washing were suspended in the 1 ml staining solution, mixed and incubated at 37° C for 15 min. The stained cells were washed twice in 1x serum free IMDM and once with 1x HBSS and resuspendend in the Fluorobrite perfusion buffer containing 0.7 mM of Ca^{2+} at the density of $0.5 – 1 \times 10^6$ cells ml^{-1}. For the two-color fluorescence imaging of the cell membrane and the selectin ligands (either CD44 or PSGL-1), the Vybrant DiO-stained KG1a cells were incubated with the Alexa-Fluor-647-conjugated anti-CD44 or anti-PSGL-1 antibodies (5 µg for each 10^6 cells) on ice for 45 min.

We used silicon rhodamine (SiR)-conjugated jasplakinolide (Cytoskeleton, Inc.) for staining actin cytoskeleton of the live KG1a cells. The harvested KG1a cells were washed three times

with 1x HBSS. The staining solution was prepared by adding 1 μl of DMSO contining1 mM of SiR-jasplakinolide and 1 μl of DMSO containing 10 mM of verapamil into 998 μl Dulbecco's modified Eagle medium (DMEM) containing 10 % bovine serum. The 10^6 cells after washing were suspended in the 1 ml staining solution, mixed and incubated at 37° C for 1 hour in presence of 5% CO_2. The stained cells were washed three times using 1x HBSS and resuspended in the Fluorobrite perfusion buffer containing 0.7 mM of Ca^{2+} at the density of 0.5 – 1 × 10^6 cells ml^{-1}. For the two-color fluorescence imaging of the actin cytoskeleton and cell membrane, the SiR-stained (i.e. actin-labeled) KG1a cells were incubated with Vybrant DiO stain at 37 ° C for 15 min.

The fluorescence imaging experiment of CD44 and cell membrane on the MβCD-treated live KG1a cells was conducted in a way similar to that on the control KG1a cells by using Vybrant DiO for the membrane stain and Alexa-Fluor-647-conjugated anti-CD44 for the immunostaining of CD44. The fluorescence labeling was conducted immediately after treating the cells with MβCD.

We used Alexa-Fluor-488-conjugated phalloidin (molecular Probes-Thermo Fisher Scientific) and anti-CD44 for staining actin cytoskeleton and CD44 of the fixed KG1a cells. The harvested KG1a cells were fixed in 3 % (w/v) paraformaldehyde (Electron Microscopy Sciences) and 0.2 % (w/v) glutaraldehyde (Electron Microscopy Sciences) in HBSS for 20 min at room temperature. The fixed cells were blocked with 10 % goat serum (Sigma) for 40 min at 37° C. The cells were then incubated with the anti-CD44 antibody (15 μg ml^{-1}) diluted in 2 % BSA in HBSS for 40 min at 37° C, followed by the Alexa-Fluor-647-conjugated goat anti-mouse secondary antibody (5 μg ml^{-1}) diluted in 2 % BSA in HBSS for 40 min at 37° C. The immunostained cells were fixed again in 3 % (w/v) paraformaldehyde and 0.2 % (w/v)

glutaraldehyde in HBSS for 10 min at room temperature. The cells were then permeabilised in 0.1 % Triton X-100 (Sigma-Aldrich) in cytoskeleton buffer (10 mM MES (pH = 6.1), 150 mM NaCl, 5 mM EGTA, 5 mM glucose, and 5 mM $MgCl_2$) for 10 min at room temperature. The permeabilised cells were labeled for actin cytoskeleton with freshly prepared 0.5 μM Alexa-Fluor-488-conjugated phalloidin in the cytoskeleton buffer containing 1 % BSA for 1 hour at room temperature. Then, the cells were fixed again in 3 % (w/v) paraformaldehyde and 0.2 % (w/v) glutaraldehyde in HBSS for 10 min at room temperature. The cells were injected into poly-L-ornithine (Sigma)-coated microfluidic chambers (ibidi GmbH, sticky-slide VI 0.4) using the syringe pump and incubated overnight at 4° C.

The fluorescence imaging experiment of CD44 on the MβCD-treated fixed KG1a cells was conducted in a way similar to that on the fixed control KG1a cells by using a combination of the anti-CD44 antibody and the Alexa-Fluor-647-conjugated anti-mouse secondary antibody(AbuZineh et al., 2018). The cells were injected into poly-L-ornithine-coated microfluidic chambers (ibidi GmbH, sticky-slide VI 0.4) using the syringe pump and incubated overnight at 4° C.

For single-molecule tracking experiment of the PSGL-1 molecules on the control live KG1a cells (i.e. not rolling cells), the cells were blocked with Fc receptor blocker (Innovex Biosciences) for 45 min on ice, then the cells were immunostained by Alexa-Fluor-488-conjugated anti-PSGL-1 for 45 min on ice at much lower concentration (20 ng for each 10^6 cells) to sparsely label the PSGL-1 molecules localized on microvilli so that the motion of individual PSGL-1 molecules can be captured. The immunostained KG1a cells were suspended in HBSS at the density of 0.5 – 1×10^6 cells ml^{-1}. Then, the cells were injected into the microfluidic chambers (ibidi GmbH, glass-slide VI 0.5).

Fluorescence imaging. Fluorescence imaging experiments were conducted using a home-built wide-field fluorescence microscopy setup (Serag et al., 2014). Continuous wave (CW) solid-state laser operating at either 488nm (60 mW, Cobolt, MLD), 532 nm (100 mW, Cobolt, Samba), or 638 nm (60 mW, Cobolt, MLD) that passed an excitation filter (Semrock, LD01-640/8, FF01-532-12.5 or FF01-488/6 for the 638 nm, 532 nm or 488 nm excitation, respectively) and a beam expander (Thorlabs) was introduced into an inverted microscope (Olympus, IX71) through a focusing lane (f = 300 mm). The laser was reflected by a dichroic mirror (Semrock, FF660-Di02-25x36, Di01-R532-25x36, or FF506-Di03-25x36 for the 638 nm, 532 nm or 488 nm excitation, respectively) and the sample was illuminated through an objective lens (Olympus, 100× NA = 1.49, UAPON 100XOTIRF, 60× NA = 1.3, UPLSAPO60XS2 or 40× NA = 1.25, UPLSAPO40XS). The excitation power was adjusted to 1 – 2 mW cm^{-2} at the sample plane using an acousto-optical tuneable filter (AOTF; AA Optoelectronics) inserted in the excitation beam pass. The fluorescence from the sample was captured by the same objective, separated from the illumination light by the same dichroic mirror, passed an emission bandpass filter (Semrock, FF01-697/58-25, FF01-580/60, or FF01-550/88 for the 638 nm, 532 nm or 488 nm excitation, respectively), and detected by an EMCCD camera (Andor Technology, iXon3 897). The fluorescence images were recorded with either 133-nm or 333-nm pixel size at 30 ms exposure time. The exposure of the EMCCD camera and the illumination of the sample by the excitation laser were synchronized by the AOTF using a laser control system (Andor Technology, PCUB-110). The image acquisition was done using the Andor iQ3 software. 3D fluorescence images were obtained by recording epi-fluorescence images of the cells at different Z-axis positions with 0.5 – 1.0 μm step size using a piezo objective scanner (PI PIFPC® P721) and reconstructing 3D images using ImageJ plugin.

Two-color fluorescence imaging experiments were conducted by introducing 638-nm and 488-nm lines of the lasers coaxially into the inverted microscope in the same way as the single-color excitation. The samples were excited through the objective lens (Olympus, 100× NA = 1.49, UAPON 100XOTIRF or 40× NA = 1.25, UPLSAPO40XS). The fluorescence from the sample was captured by the same objective, separated from the illumination light by a multiband dichroic mirror (Semrock, Di03-405/488/561/635-t1-25x36), and passed through a TuCam dual-camera adaptor (Andor Technology) equipped with a filter cassette containing a dichroic mirror (Semrock, FF580-FDi01-25x36) to separate the fluorescence into two channels. The separated fluorescence from the samples was detected by two EMCCD cameras (Andor Technology, iXon3 897) through emission bandpass filters (Semrock, FF01-550/88-25 and FF01-697/58-25).

Determination of the number of PSGL-1 molecules on tethers and slings. The number of PSGL-1 molecules in each spot on the tethers and slings formed during KG1a cells rolling over E-selectin was calculated by comparing the integrated fluorescence intensity obtained from each PSGL-1 spot with the intensity obtained from single Alexa-Fluor-dye-conjugated anti-PSGL-1 antibody. To determine the fluorescence intensity obtained from single Alexa-Fluor-dye-conjugated anti-PSGL-1 antibody, the antibody was deposited on the surface of the microfluidic chamber at a concentration of 0.02 $\mu g\ ml^{-1}$. Fluorescence signals from the single deposited antibodies were captured at the experimental conditions identical to those for the imaging experiment on the immunostained KG1a cells rolling over E-selectin. We used only well-focused fluorescence images of the PSGL-1 spots on the tethers and slings for this analysis to ensure an accurate estimation of the number of the PSGL-1 molecules.

Single-molecule tracking analysis. Single-molecule tracking analysis of the PSGL-1 molecules moving along the tethers and slings of KG1a cells rolling over E-selectin and localized on the microvilli of control KG1a cells were conducted by generating single-molecule diffusion trajectories using a versatile tracking algorithm (Jaqaman et al., 2008; Serag and Habuchi, 2017). The algorithm uses a mixture-model fitting algorithm to localize and track multiple particles in the same field of view. It can detect the merging and splitting of particles during motion. To achieve these tracking targets, the algorithm localizes and tracks all the local maxima in the single-molecule image including maxima that are partially overlapping along the tethers and slings. The diffusion rate (i.e. diffusion coefficient) and mode were analyzed by mean square displacement (MSD) analysis (Kusumi et al., 1993). The MSD was calculated from the generated diffusion trajectories by using equation (3)

$$MSD(\Delta t) = \langle (x_{i+n} - x_i)^2 + (y_{i+n} - y_i)^2 \rangle, \quad (3)$$

where x_{i+n} and y_{i+n} demote the spatial positions after time interval Δt, given by the frame number, n, after starting at positions x_i and y_i. . The MSD-Δt profiles were fitted to random (equation (4)), and confined (equation (5)) diffusion models.

$$MSD(\Delta t) = 4D\Delta t, \quad (4)$$

where D is the diffusion coefficient,

$$MSD = \frac{L^2}{3}\left[1 - \exp\left(\frac{-12D\Delta t}{L^2}\right)\right], \quad (5)$$

where L is the side length of the confined area.

Super-resolution fluorescence imaging and analysis. Super-resolution (SR) fluorescence localization microscopy imaging of fixed immunolabeled KG1a cells was performed in an imaging buffer composed of TN buffer (50 mM tris (pH 8.0) and 10 mM NaCl), oxygen scavenging system (glucose oxidase (0.5 mg ml^{-1}, Sigma), catalase (40 μg ml^{-1}, Sigma), 10% (w/v) glucose), and 100 mM β-mercaptoethanol (Sigma) as a reducing reagent. The imaging solution was prepared immediately before the imaging experiments. The imaging experiments were conducted on a custom-built wide-field illumination fluorescence microscope on an inverted optical microscope platform described above (Abadi et al., 2018; AbuZineh et al., 2018). The fluorescence images were recorded using a 150 × 150 pixel region of the EMCCD camera with 83-nm pixel size at 10-ms exposure time. The fluorescence image sequences with 10,000 frames were recorded for the reconstruction of SR localization microscopy images.

The SR images were reconstructed by using either a custom-written MATLAB (MathWorks) code or Localizer software (Dedecker et al., 2012). The positions of the AF-647 molecules were determined by 2D Gaussian fitting of the images. We removed fluorescence spots whose width was significantly larger (>200 nm) than the point spread function (PSF) of the optical system (PSF, ~130 nm) from the analysis. The effect of the stage drift in the *xy* plane was corrected by reconstructing the subimages using 5000 localizations. In the two-color SR imaging, TetraSpeck microspheres (diameter, 100 nm) deposited on a cleaned coverslip was used to calibrate the shift between the two channels. Using fluorescence images of the TetraSpeck microspheres recorded simultaneously on the two cameras, we generated a registration map that corrects the shift between the two images and applied the registration map to the images obtained from the cell samples.

Scanning electron microscopy. The harvested KG1a cells (10^7 cells) were washed twice with HBSS. The cells were fixed in 2-2.5% glutaraldehyde in 0.1 M Cacodylate buffer (pH = 7.2 – 7.4) in 4°C for overnight. The fixed cells were washed three times with the 0.1 M Cacodylate buffer with 15 min submerged in buffer before the next wash and resuspended in the 200 µl of the buffer. Then, 100 µl of the cell suspension was added on a cover slip, which was brushed with polylysine and incubated overnight inside a moisturized chamber before use. The cells were further fixed in 1% osmium tetroxide in 0.1 M Cacodylate buffer for one hour in dark. The cells were washed three times with distilled water, where they were submerged in water for 15 min before the next wash, and dehydrated in gradient ethanol (30, 50, 70, 90 and 100 %). Samples were carried further onto Critical Point Drying apparatus and covered with 100 % ethanol to completely submerge the samples. The dehydrated cells were placed on a holder of the scanning electron microscope (SEM) and coated with 4mm platinum (K575X Sputter Coater, Quorum). The SEM images were recorded using Teneo SEM (Thermo Fischer).

Flow cytometry. Binding specificity of the mouse anti-human PSGL-1 and mouse anti-human CD44 antibodies, which were used for the fluorescence imaging experiments, to PSGL-1 and CD44 on KG1a cells were evaluated by flow cytometry. KG1a cells (10^6 cells ml^{-1}) were incubated with either anti-human PSGL-1 antibody (clone KPL-1, Ms IgG1, $_\kappa$), anti-human CD44 antibody (clone 515 Ms IgG1, $_\kappa$, or 2C5 Ms IgG2a) or purified mouse IgG1κ isotype (BioLegend) at a final concentration of 10 µg ml^{-1} in HBSS at 4°C for 30 min. Subsequently, the KG1a cells were incubated with Alexa-Fluor-488–conjugated goat anti-mouse antibody (5 µg ml^{-1}, IgG, Invitrogen) in HBSS at 4°C for 20 min. For the secondary antibody control, KG1a cells (10^6 cells ml^{-1}) were incubated with Alexa-Fluor-488–conjugated goat anti-mouse antibody (5 µg ml^{-1}) in HBSS at 4°C

for 20 min. The fluorescence intensity was determined using a FACSCanto flow cytometer (Beckman Dickenson).

Western Blot Analysis. WT KG1a, scrambled, or CD34 siRNA knockdown cells were lysed using a cell lysis buffer containing 88% NP40 (Invitrogen™ Novex™, Fisher Scientific), 10% protease inhibitor (Pierce™, Thermo Scientific), 1% PMSF, and 1% Phosphatase inhibitor (Halt™, Thermo Scientific) at 4°C for 1 h. The whole cell lysate was collected and incubated with NuPAGE LDS sample buffer (Invitrogen) and 10% β-mercaptoethanol at 70°C for 10 min. The samples were then run on an SDS-PAGE gel prior to being transferred to a PVDF membrane. The PVDF membrane was blocked overnight at 4°C using Tris-buffered saline with Tween-20 (Cell Signaling Technology) containing 5% non-fat skim milk powder. The membrane was then washed and incubated with a mouse anti-human CD34 antibody (QBEND/10, BIO RAD). The membrane was then washed and immunoblotted with HRP-conjugated secondary antibodies prior to imaging.

Supplemental Information titles

Figure S1. Experimental design.

Figure S2. Spatiotemporal behavior of tethers and slings.

Figure S3. Spatial colocalization of PSGL-1 with membrane tethers/slings and CD44.

Figure S4. 3D views of the tethers and slings formed on a KG1a cell that demonstrates clustering behavior of PSGL-1 at the tethering points during cell rolling over E-selectin.

Figure S5. Scanning electron microscopy (SEM) images of KG1a cells.

Figure S6. Effect of the knockdown of CD34 on the formation of tethers and slings on KG1a cells while rolling over E-selectin.

Figure S7. Single-molecule tracking analysis of PSGL-1 on KG1a cells.

Video S1. Time-lapse fluorescence images of CD44 on a KG1a cell perfused into a microfluidic chamber at a shear stress of 1 – 8 dyne cm^{-2}.

Video S2. Time-lapse fluorescence images of CD44 on a KG1a cell perfused into a microfluidic chamber that shows the conversion of a tether into sling.

Video S3. Time-lapse fluorescence images of CD44 on a KG1a cell perfused into a microfluidic chamber that shows the retraction of the sling.

Video S4. Time-lapse fluorescence images of PSGL-1 on a KG1a cell perfused into a microfluidic chamber that shows the discrete spatial distribution of the PSGL-1 molecules on the tether.

Video S5. Time-lapse fluorescence images of PSGL-1 on a KG1a cell perfused into a microfluidic chamber that shows the discrete spatial distribution of the PSGL-1 molecules on the sling.

Video S6. Time-lapse fluorescence images of CD44 on KG1a cells perfused into a microfluidic chamber that shows the formation of the tethers and slings on all the rolling cells.

Video S7. Time-lapse fluorescence images of PSGL-1 on a KG1a cell perfused into a microfluidic chamber that shows the merger of multiple tethers.

References

Abadi, M., Serag, M.F., and Habuchi, S. (2018). Entangled polymer dynamics beyond reptation. Nat Commun *9*, 5098.

Abbal, C., Lambelet, M., Bertaggia, D., Gerbex, C., Martinez, M., Arcaro, A., Schapira, M., and Spertini, O. (2006). Lipid raft adhesion receptors and Syk regulate selectin-dependent rolling under flow conditions. Blood *108*, 3352-3359.

AbuSamra, D.B., Al-Kilani, A., Hamdan, S.M., Sakashita, K., Gadhoum, S.Z., and Merzaban, J.S. (2015). Quantitative characterization of E-selectin interaction with native CD44 and P-selectin glycoprotein ligand-1 (PSGL-1) using a real time immunoprecipitation-based binding assay. J Biol Chem *290*, 21213-21230.

AbuSamra, D.B., Aleisa, F.A., Al-Amoodi, A.S., Jalal Ahmed, H.M., Chin, C.J., Abuelela, A.F., Bergam, P., Sougrat, R., and Merzaban, J.S. (2017). Not just a marker: CD34 on human hematopoietic stem/progenitor cells dominates vascular selectin binding along with CD44. Blood Adv *1*, 2799-2816.

AbuZineh, K., Joudeh, L.I., Al Alwan, B., Hamdan, S.M., Merzaban, J.S., and Habuchi, S. (2018). Microfluidics-based super-resolution microscopy enables nanoscopic characterization of blood stem cell rolling. Sci Adv *4*, eaat5304.

Alon, R., Hammer, D.A., and Springer, T.A. (1995). Lifetime of the P-selectin-carbohydrate bond and its response to tensile force in hydrodynamic flow. Nature *374*, 539-542.

Cai, E., Marchuk, K., Beemiller, P., Beppler, C., Rubashkin, M.G., Weaver, V.M., Gerard, A., Liu, T.L., Chen, B.C., Betzig, E.*, et al.* (2017). Visualizing dynamic microvillar search and stabilization during ligand detection by T cells. Science *356*, 10.

Chen, S.Q., and Springer, T.A. (1999). An automatic braking system that stabilizes leukocyte rolling by an increase in selectin bond number with shear. J Cell Biol *144*, 185-200.

Cummings, R.D., and McEver, R.P. (2009). C-type lectins. In Essentials of glycobiology, A. Varki, R.D. Cummings, J.D. Esko, H.H. Freeze, P. Stanley, C.R. Bertozzi, G.W. Hart, and M.E. Etzler, eds. (Cold Spring Harbor (NY): Cold Spring Harbor Laboratory Press).

Dedecker, P., Duwe, S., Neely, R.K., and Zhang, J. (2012). Localizer: fast, accurate, open-source, and modular software package for superresolution microscopy. J Biomed Opt *17*, 5.

Dimitroff, C.J., Lee, J.Y., Rafii, S., Fuhlbrigge, R.C., and Sackstein, R. (2001). CD44 is a major E-selectin ligand on human hematopoietic progenitor cells. J Cell Biol *153*, 1277-1286.

Evans, E., Heinrich, V., Leung, A., and Kinoshita, K. (2005). Nano- to microscale dynamics of P-selectin detachment from leukocyte interfaces. I. Membrane separation from the cytoskeleton. Biophys J *88*, 2288-2298.

Frenette, P.S., Subbarao, S., Mazo, I.B., von Andrian, U.H., and Wagner, D.D. (1998). Endothelial selectins and vascular cell adhesion molecule-1 promote hematopoietic progenitor homing to bone marrow. Proc Natl Acad Sci U S A *95*, 14423-14428.

Gaborski, T.R., Clark, A., Waugh, R.E., and McGrath, J.L. (2008). Membrane Mobility of beta 2 Integrins and Rolling Associated Adhesion Molecules in Resting Neutrophils. Biophys J *95*, 4934-4947.

Goetz, D.J., Greif, D.M., Ding, H., Camphausen, R.T., Howes, S., Comess, K.M., Snapp, K.R., Kansas, G.S., and Luscinskas, F.W. (1997). Isolated P-selectin glycoprotein ligand-1 dynamic adhesion to P- and E-selectin. J Cell Biol *137*, 509-519.

Gopalakrishnan, M., Forsten-Williams, K., Nugent, M.A., and Tauber, U.C. (2005). Effects of receptor clustering on ligand dissociation kinetics: Theory and simulations. Biophys J *89*, 3686-3700.

Hanley, W.D., Wirtz, D., and Konstantopoulos, K. (2004). Distinct kinetic and mechanical properties govern selectin-leukocyte interactions. J Cell Sci *117*, 2503-2511.

Heinrich, V., Leung, A., and Evans, E. (2005). Nano- to microscale dynamics of P-selectin detachment from leukocyte interfaces. II. Tether flow terminated by P-selectin dissociation from PSGL-1. Biophys J *88*, 2299-2308.

Hidalgo, A., Weiss, L.A., and Frenette, P.S. (2002). Functional selectin ligands mediating human CD34(+) cell interactions with bone marrow endothelium are enhanced postnatally. J Clin Invest *110*, 559-569.

Hocde, S.A., Hyrien, O., and Waugh, R.E. (2009). Cell Adhesion Molecule Distribution Relative to Neutrophil Surface Topography Assessed by TIRFM. Biophys J *97*, 379-387.

Jaqaman, K., Loerke, D., Mettlen, M., Kuwata, H., Grinstein, S., Schmid, S.L., and Danuser, G. (2008). Robust single-particle tracking in live-cell time-lapse sequences. Nat Methods *5*, 695-702.

Kolaczkowska, E., and Kubes, P. (2013). Neutrophil recruitment and function in health and inflammation. Nat Rev Immunol *13*, 159-175.

Kusumi, A., Sako, Y., and Yamamoto, M. (1993). Confined lateral diffusion of membrane receptors as studied by single particle tracking (nanovid microscopy). Effects of calcium-induced differentiation in cultured epithelial cells. Biophys J *65*, 2021-2040.

Lehr, J.E., and Pienta, K.J. (1998). Preferential adhesion of prostate cancer cells to a human bone marrow endothelial cell line. J Natl Cancer Inst *90*, 118-123.

Ley, K., Hoffman, H.M., Kubes, P., Cassatella, M.A., Zychlinsky, A., Hedrick, C.C., and Catz, S.D. (2018). Neutrophils: New insights and open questions. Sci Immunol *3*, 14.

Ley, K., Laudanna, C., Cybulsky, M.I., and Nourshargh, S. (2007). Getting to the site of inflammation: the leukocyte adhesion cascade updated. Nat Rev Immunol *7*, 678-689.

Lukinavicius, G., Reymond, L., D'Este, E., Masharina, A., Gutfert, F., Ta, H., Guether, A., Fournier, M., Rizzo, S., Waldmann, H.*, et al.* (2014). Fluorogenic probes for live-cell imaging of the cytoskeleton. Nat Methods *11*, 731-U168.

Magnon, C., and Frenette, P.S. (2008). Hematopoietic stem cell trafficking. In StemBook.

Marki, A., Gutierrez, E., Mikulski, Z., Groisman, A., and Ley, K. (2016). Microfluidics-based side view flow chamber reveals tether-to-sling transition in rolling neutrophils. Sci Rep *6*, 8.

Marshall, B.T., Long, M., Piper, J.W., Yago, T., McEver, R.P., and Zhu, C. (2003). Direct observation of catch bonds involving cell-adhesion molecules. Nature *423*, 190-193.

Mazo, I.B., Gutierrez-Ramos, J.C., Frenette, P.S., Hynes, R.O., Wagner, D.D., and von Andrian, U.H. (1998). Hematopoietic progenitor cell rolling in bone marrow microvessels: Parallel contributions by endothelial selectins and vascular cell adhesion molecule 1. J Exp Med *188*, 465-474.

McEver, R.P., and Zhu, C. (2010). Rolling cell adhesion. Annu Rev Cell Dev Biol *26*, 363-396.

Merzaban, J.S., Burdick, M.M., Gadhoum, S.Z., Dagia, N.M., Chu, J.T., Fuhlbrigge, R.C., and Sackstein, R. (2011). Analysis of glycoprotein E-selectin ligands on human and mouse marrow cells enriched for hematopoietic stem/progenitor cells. Blood *118*, 1774-1783.

Miner, J.J., Xia, L., Yago, T., Kappelmayer, J., Liu, Z., Klopocki, A.G., Shao, B., McDaniel, J.M., Setiadi, H., Schmidtke, D.W.*, et al.* (2008). Separable requirements for cytoplasmic domain of PSGL-1 in leukocyte rolling and signaling under flow. Blood *112*, 2035-2045.

Moore, K.L., Patel, K.D., Bruehl, R.E., Li, F.G., Johnson, D.A., Lichenstein, H.S., Cummings, R.D., Bainton, D.F., and McEver, R.P. (1995). P-selectin glycoprotein ligand-1 mediates rolling of human neutrophils on P-selectin. J Cell Biol *128*, 661-671.

Murphy, D.B., and Davidson, M.W. (2012). Fundamental of light microscopy and electronic imaging (Wiley-Blackwell).

Ponta, H., Sherman, L., and Herrlich, P.A. (2003). CD44: From adhesion molecules to signalling regulators. Nat Rev Mol Cell Biol *4*, 33-45.

Quail, D.F., and Joyce, J.A. (2013). Microenvironmental regulation of tumor progression and metastasis. Nat Med *19*, 1423-1437.

Schmidt, B.J., Papin, J.A., and Lawrence, M.B. (2009). Nano-motion Dynamics are Determined by Surface-Tethered Selectin Mechanokinetics and Bond Formation. PLoS Comput Biol *5*, 19.

Schmidtke, D.W., and Diamond, S.L. (2000). Direct observation of membrane tethers formed during neutrophil attachment to platelets or P-selectin under physiological flow. J Cell Biol *149*, 719-729.

Schweitzer, K.M., Drager, A.M., vanderValk, P., Thijsen, S.F.T., Zevenbergen, A., Theijsmeijer, A.P., vanderSchoot, C.E., and Langenhuijsen, M. (1996). Constitutive expression of E-selectin and vascular cell adhesion molecule-1 on endothelial cells of hematopoietic tissues. Am J Pathol *148*, 165-175.

Serag, M.F., Abadi, M., and Habuchi, S. (2014). Single-molecule diffusion and conformational dynamics by spatial integration of temporal fluctuations. Nat Commun *5*, 10.

Serag, M.F., and Habuchi, S. (2017). Conserved linear dynamics of single-molecule Brownian motion. Nat Commun *8*, 15675.

Setiadi, H., and McEver, R.P. (2008). Clustering endothelial E-selectin in clathrin-coated pits and lipid rafts enhances leukocyte adhesion under flow. Blood *111*, 1989-1998.

Shao, B.J., Yago, T., Setiadi, H., Wang, Y., Mehta-D'souza, P., Fu, J.X., Crocker, P.R., Rodgers, W., Xia, L.J., and McEver, R.P. (2015). O-glycans direct selectin ligands to lipid rafts on leukocytes. Proc Natl Acad Sci U S A *112*, 8661-8666.

Shao, J.Y., Ting-Beall, H.P., and Hochmuth, R.M. (1998). Static and dynamic lengths of neutrophil microvilli. Proc Natl Acad Sci U S A *95*, 6797-6802.

Snapp, K.R., Heitzig, C.E., and Kansas, G.S. (2002). Attachment of the PSGL-1 cytoplasmic domain to the actin cytoskeleton is essential for leukocyte rolling on P-selectin. Blood *99*, 4494-4502.

Sundd, P., Gutierrez, E., Koltsova, E.K., Kuwano, Y., Fukuda, S., Pospieszalska, M.K., Groisman, A., and Ley, K. (2012). 'Slings' enable neutrophil rolling at high shear. Nature *488*, 399-403.

Sundd, P., Pospieszalska, M.K., and Ley, K. (2013). Neutrophil rolling at high shear: Flattening, catch bond behavior, tethers and slings. Mol Immunol *55*, 59-69.

Wang, Y., Yago, T., Zhang, N., Abdisalaam, S., Alexandrakis, G., Rodgers, W., and McEver, R.P. (2014). Cytoskeletal Regulation of CD44 Membrane Organization and Interactions with E-selectin. J Biol Chem *289*, 35159-35171.

Yago, T., Fu, J.X., McDaniel, J.M., Miner, J.J., McEver, R.P., and Xia, L.J. (2010a). Core 1-derived O-glycans are essential E-selectin ligands on neutrophils. Proc Natl Acad Sci U S A *107*, 9204-9209.

Yago, T., Shao, B.J., Miner, J.J., Yao, L.B., Klopocki, A.G., Maeda, K., Coggeshall, K.M., and McEver, R.P. (2010b). E-selectin engages PSGL-1 and CD44 through a common signaling pathway to induce integrin alpha(L)beta(2)-mediated slow leukocyte rolling. Blood *116*, 485-494.

Supplemental Information

Supplemental Figures

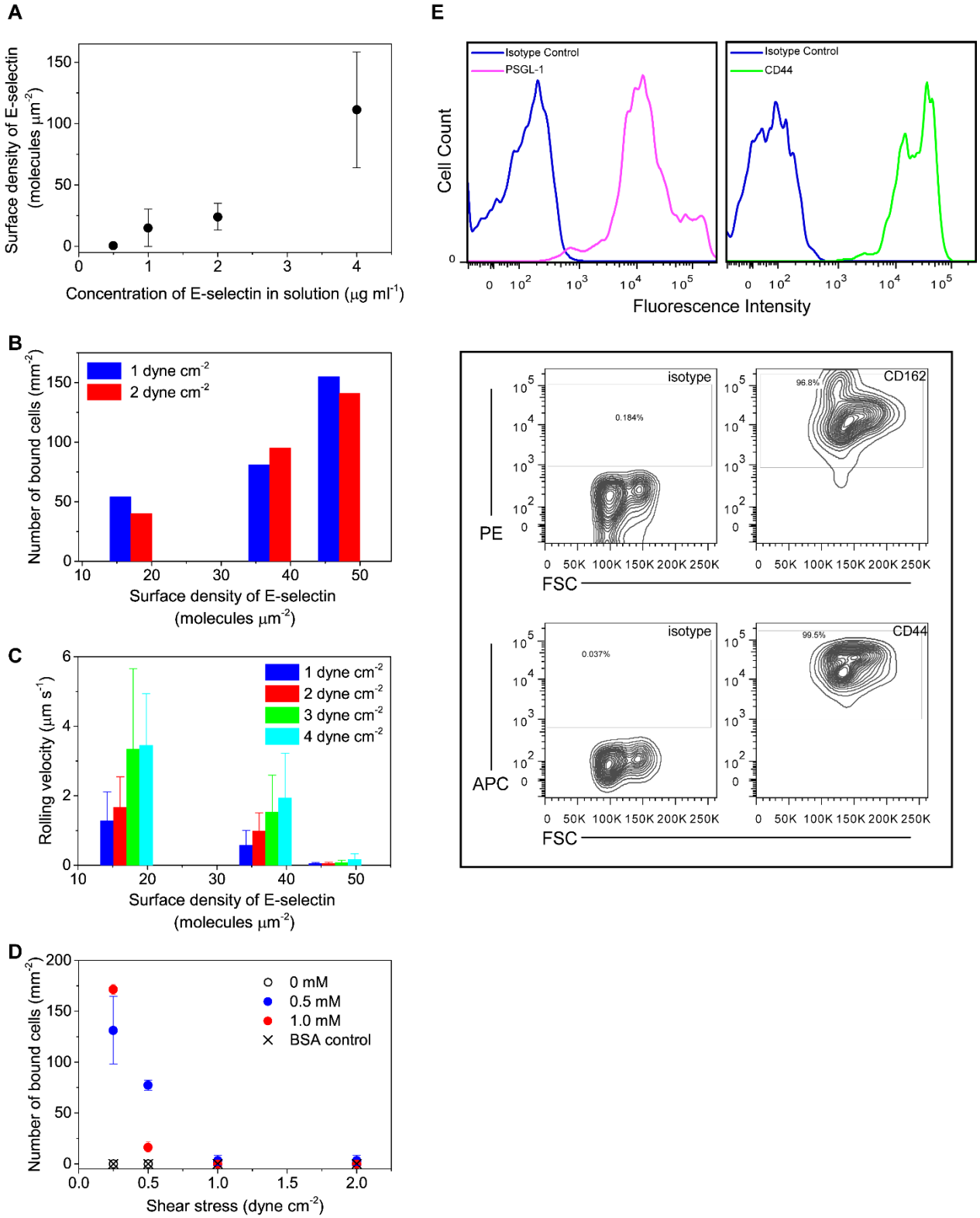

Figure S1. Experimental design. (A)Surface density of rh E-selectin molecules. The surface densities of the rh E-selectin molecules were determined after incubating the microfluidic chambers with HBSS buffer containing different concentrations of the recombinant E-selectin at 4 °C overnight. The error bars show the standard deviations determined by at least four separate experiments. (B) Characterization of the rolling behavior of KG1a cells on E-selectin. Number of bound cells to the E-selectin surface at different surface densities of the deposited rh E-selectin. The cells were injected into the microfluidic chambers at the shear stresses of either 1 or 2 dyne cm^{-2}. (C) Rolling velocity of the cells on the E-selectin surface at different surface densities of the deposited rh E-selectin. The cells were injected into the microfluidic chambers at the shear stresses of either 1, 2, 3 or 4 dyne cm^{-2}. The error bars show the standard deviations determined by at least six separate experiments. (D) Number of bound cells to the E-selectin surface at different applied shear stresses. The cells were injected into the microfluidic chambers at the calcium ion concentrations of either 0, 0.5 or 1.0 mM. BSA control (i.e. no E-selectin on the surface) is included as a negative control. The error bars show the standard deviations determined by at least three separate experiments. (E) Assessment of E-selectin ligand expression on human $CD34^{pos}$-HSPCs. Primary human $CD34^{pos}$-HSPCs were stained for CD44 (green) and PSGL-1 (magenta) using antibodies specific to these antigens (anti-human CD44, clone 2C5 and anti-human PSGL-1, clone KPL-1) and analyzed by flow cytometry (FACS Canto and FlowJo). This is a representative experiment of n=2 independent experiments.

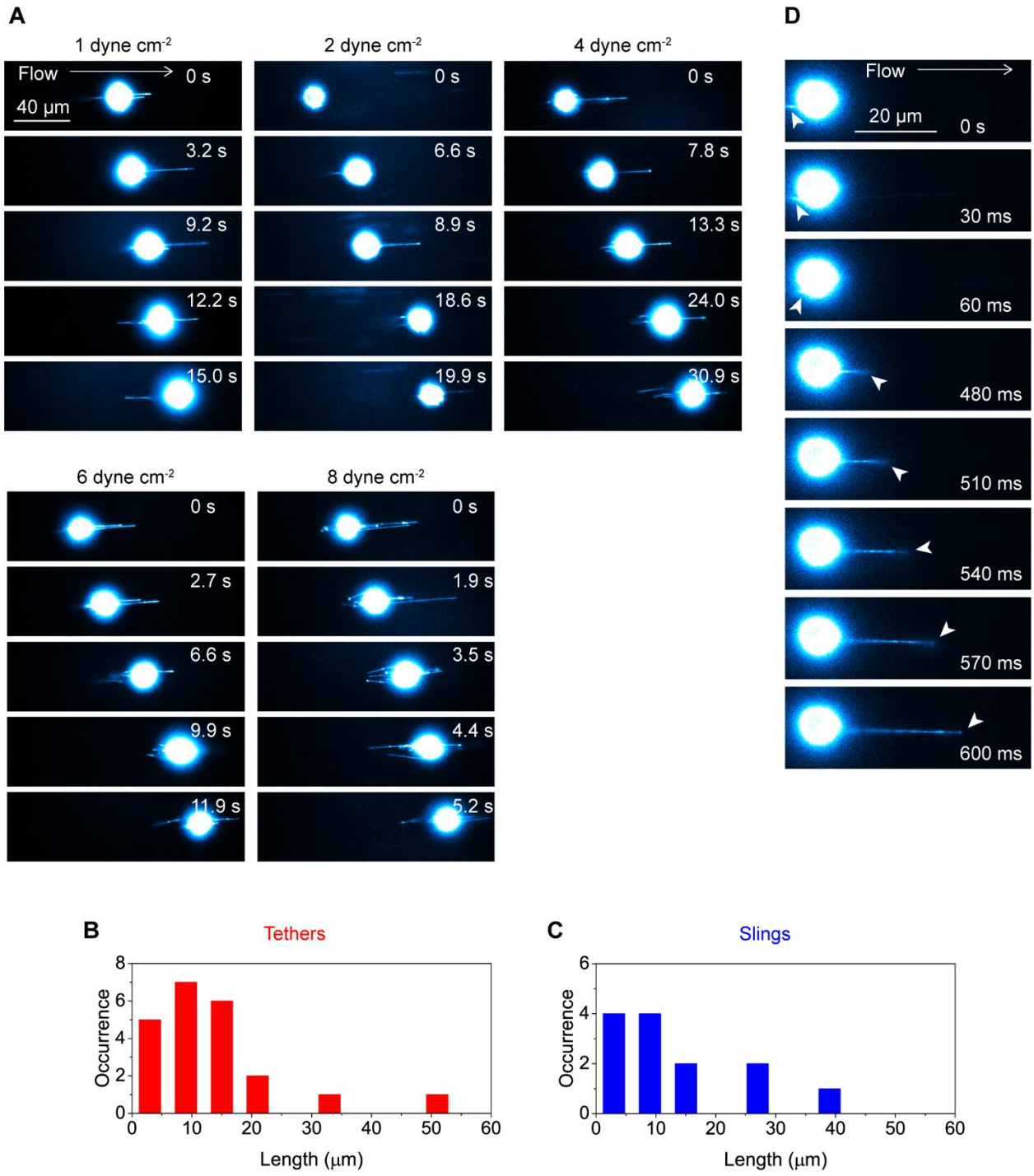
A
1 dyne cm-2
2 dyne cm-2
4 dyne cm-2
Flow
40 μm
0 s
3.2 s
9.2 s
12.2 s
15.0 s
6.6 s
8.9 s
18.6 s
19.9 s
7.8 s
13.3 s
24.0 s
30.9 s
6 dyne cm-2
8 dyne cm-2
2.7 s
6.6 s
9.9 s
11.9 s
1.9 s
3.5 s
4.4 s
5.2 s
D
20 μm
30 ms
60 ms
480 ms
510 ms
540 ms
570 ms
600 ms
B
Tethers
Occurrence
Length (μm)
C
Slings

Figure S2. Spatiotemporal behavior of tethers and slings. (A) Shear force-dependent formation of the tethers and slings on KG1a cells rolling over E-selectin. Time-lapse fluorescence images of CD44 (immunostained by Alexa-Fluor-647-conjugated anti-CD44 antibody) captured during cell rolling over the surface-deposited E-selectin molecules. The labeled cells were injected into the microfluidic chambers whose surface was coated with rh E-selectin molecules at a density of 15 molecules μm^{-2}. The cells were injected into the chambers at a shear stress of 1, 2, 4 or 8 dyne cm^{-2}. (B) Length of the tethers formed on primary human $CD34^{pos}$-HSPCs rolling over E-selectin. Frequency histogram of the length of tethers formed during the primary human $CD34^{pos}$-HSPCs rolling over E-selectin. The cells were injected into the microfluidic chambers whose surface was coated with rh E-selectin molecules at a density of 15 molecules μm^{-2}. The cells were injected into the chambers at a shear stress of 2 dyne cm^{-2} as indicated. (C) Length of the slings formed on primary human $CD34^{pos}$-HSPCs rolling over E-selectin. Frequency histogram of the length of slings formed during the primary human $CD34^{pos}$-HSPCs rolling over E-selectin. The cells were injected into the microfluidic chambers whose surface was coated with rh E-selectin molecules at a density of 15 molecules μm^{-2}. The cells were injected into the chambers at a shear stress of 2 dyne cm^{-2} as indicated. (D) Conversion of a tether into sling observed for a primary human $CD34^{pos}$-HSPC rolling over E-selectin. Time-lapse fluorescence images of CD44 (immunostained by Alexa-Fluor-647-conjugated anti-CD44 antibody) captured during cell rolling over the surface-deposited E-selectin molecules. The arrow heads show the tether that is converted into sling upon the detachment of the tethering point from the E-selectin surface. The cells were injected into the microfluidic chambers whose surface was coated with rh E-selectin molecules at a density of 15 molecules μm^{-2}. The cells were injected into the chambers at a shear stress of 2 dyne cm^{-2}.

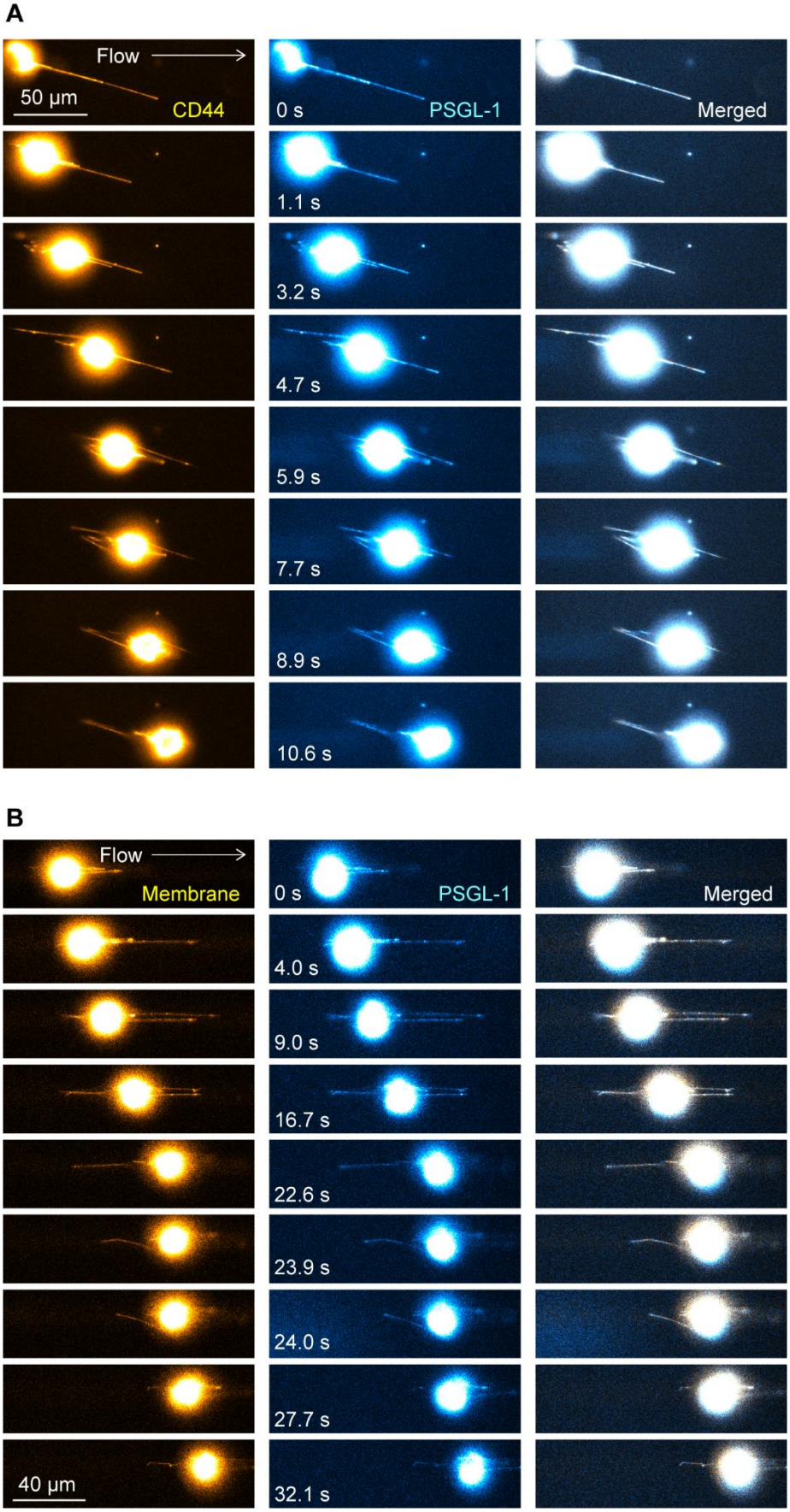
A
Flow
50 µm
CD44
0 s
PSGL-1
Merged
1.1 s
3.2 s
4.7 s
5.9 s
7.7 s
8.9 s
10.6 s
B
Flow
Membrane
0 s
PSGL-1
Merged
4.0 s
9.0 s
16.7 s
22.6 s
23.9 s
24.0 s
27.7 s
40 µm
32.1 s

Figure S3. Spatial colocalization of PSGL-1 with membrane tethers/slings and CD44. (A) Colocalization of CD44 and PSGL-1 on the tethers and slings formed on a KG1a cell rolling over E-selectin. Time-lapse fluorescence images of CD44 (yellow, immunostained by Alexa-Fluor-647-conjugated anti-CD44 antibody) and PSGL-1 (cyan, immunostained by Alexa-Fluor-488-conjugated anti-PSGL-1 antibody) captured during cell rolling over the surface-deposited E-selectin molecules. The merged images are displayed in the right panels. The labeled cells were injected into the microfluidic chambers whose surface was coated with rh E-selectin molecules at a density of 15 molecules μm^{-2}. The cells were injected into the chambers at a shear stress of 2 dyne cm^{-2}. (B) Colocalization of cell membrane and PSGL-1 on the tethers and slings formed on a KG1a cell rolling over E-selectin. Time-lapse fluorescence images of the cell membrane (yellow, stained by Vybrant DiO dye) and PSGL-1 (cyan, immunostained by Alexa-Fluor-647-conjugated anti-PSGL-1 antibody) captured during cell rolling over the surface-deposited E-selectin molecules. The merged images are displayed in the right panels. The stained and labeled cells were injected into the microfluidic chambers whose surface was coated with rh E-selectin molecules at a density of 15 molecules μm^{-2}. The cells were injected into the chambers at a shear stress of 2 dyne cm^{-2}.

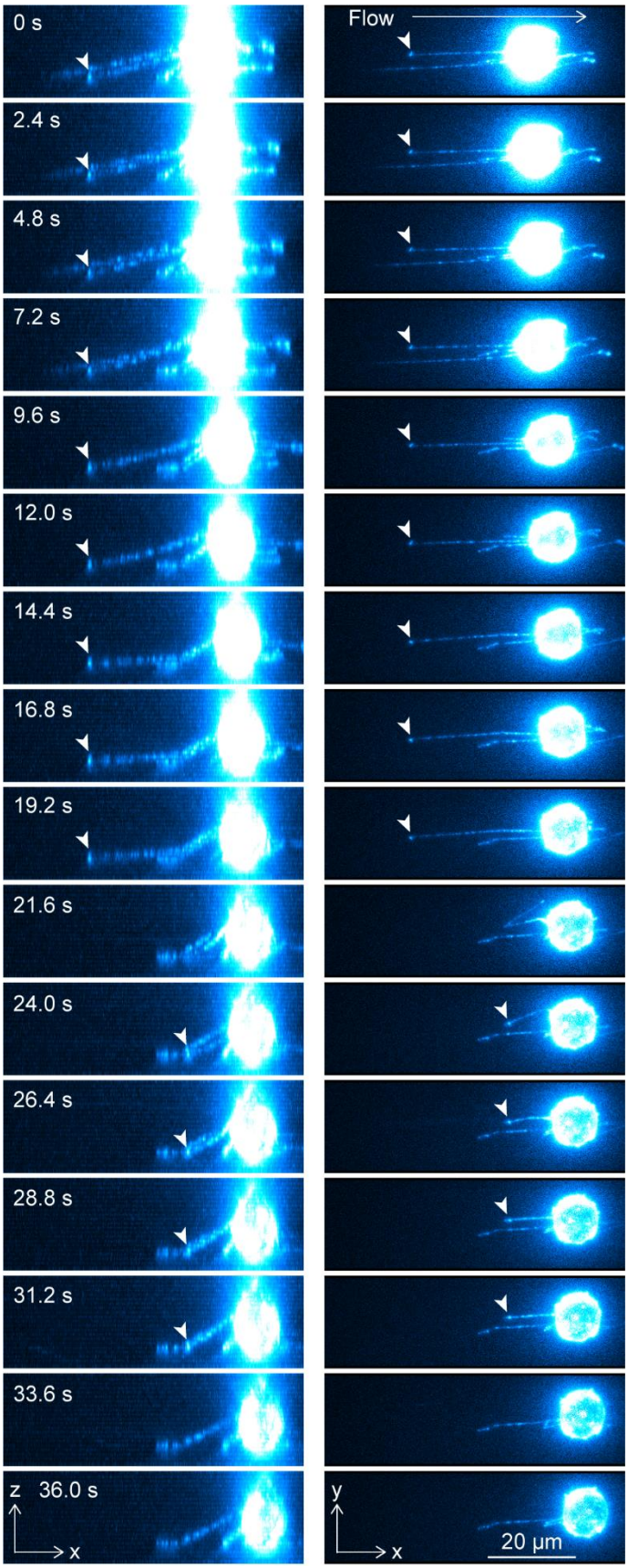
0 s
2.4 s
4.8 s
7.2 s
9.6 s
12.0 s
14.4 s
16.8 s
19.2 s
21.6 s
24.0 s
26.4 s
28.8 s
31.2 s
33.6 s
z 36.0 s
x
Flow
y
x
20 µm

Figure S4. 3D views of the tethers and slings formed on a KG1a cell that demonstrates clustering behavior of PSGL-1 at the tethering points during cell rolling over E-selectin. Side view (left) and top view (right) of the 3D reconstructed time-lapse fluorescence images of PSGL-1 (immunostained by Alexa-Fluor-555-conjugated anti-PSGL-1 antibody) captured during cell rolling over the surface-deposited E-selectin molecules. The 3D images were reconstructed by recording fluorescence images of the cell at 40 different Z-axis positions with 1.0 μm step size. The single 3D images were therefore captured every 1.2 sec (30 ms exposure time at each Z-position). The arrowheads show the bright fluorescence spots of PSGL-1 (i.e. clusters of PSGL-1) found at the tethering points. The labeled cells were injected into the microfluidic chambers whose surface was coated with rh E-selectin molecules at a density of 15 molecules μm^{-2}. The cells were injected into the chambers at a shear stress of 2 dyne cm^{-2}.

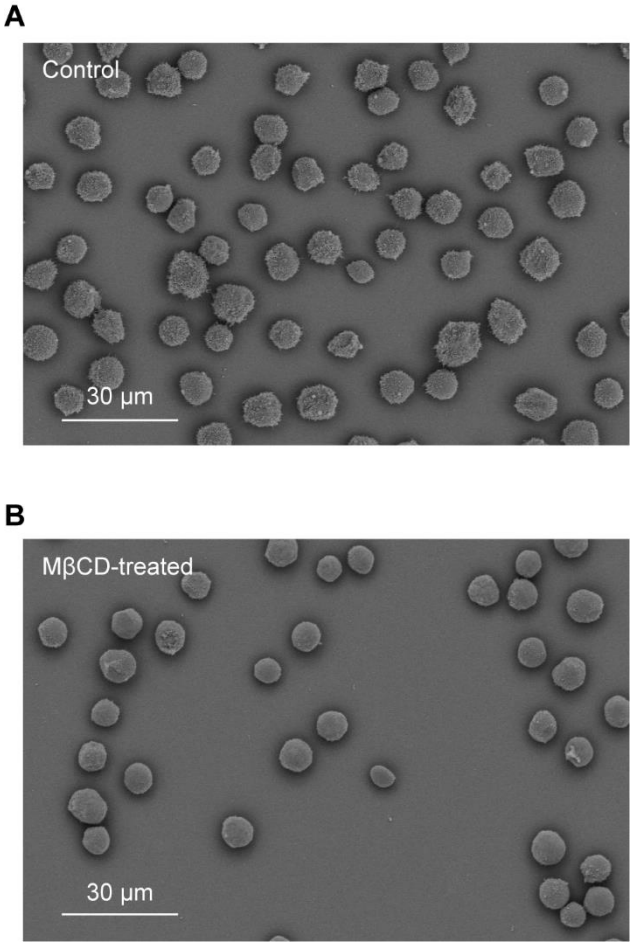

Figure S5. Scanning electron microscopy (SEM) images of KG1a cells. SEM images of (A) control and (B) methyl-β-cyclodextrin (MβCD)-treated KG1a cells. These are representative images of n=2 independent experiments.

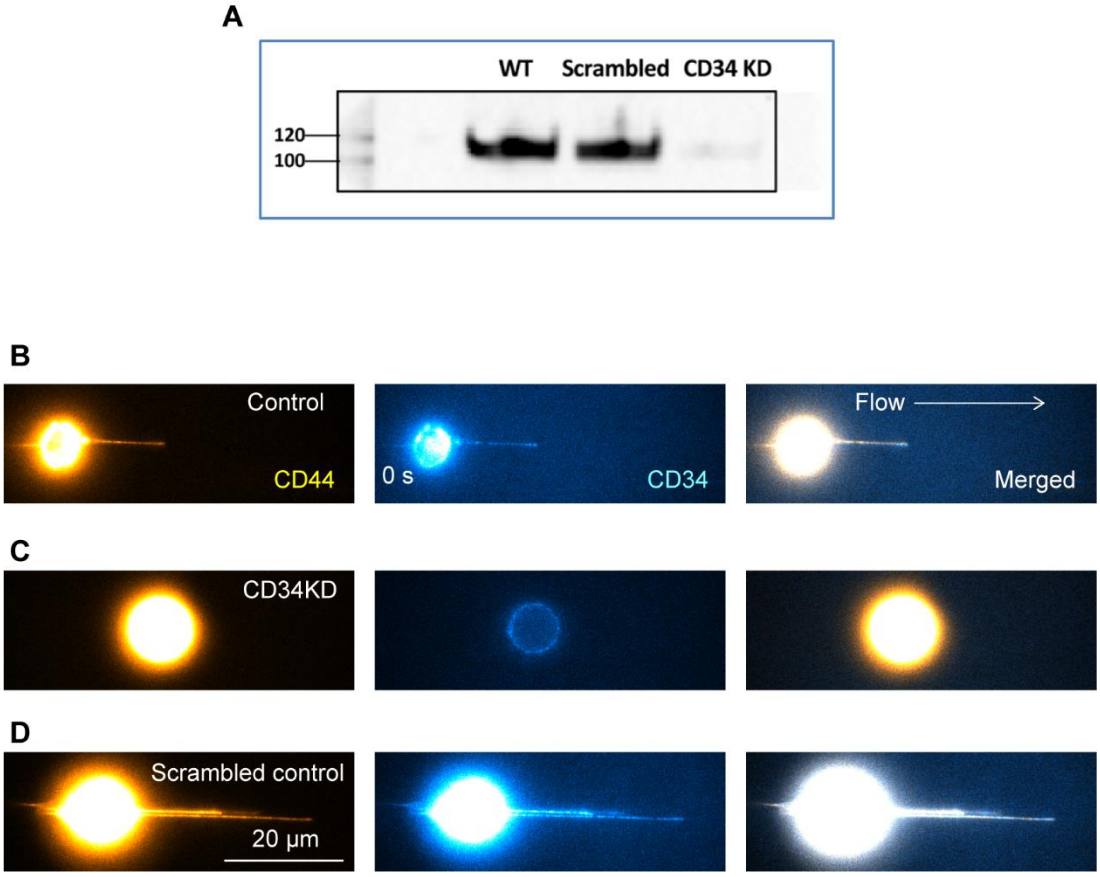

Figure S6. Effect of the knockdown of CD34 on the formation of tethers and slings on KG1a cells while rolling over E-selectin. (A) CD34 knockdown in KG1a cells. KG1a cells were transfected with either a scrambled control siRNA (Silencer Select, Life technologies; 4390843) or with siRNA specific for CD34 (Select, Life technologies; 4392420-s2644). Cells were collected after 48 h of transfection and subjected to Western blot analysis for CD34 protein expression. Lane 1: untreated KG1a cells; Lane 2: scrambled negative control siRNA; Lane 3: CD34 KD KG1a cells. Membrane bands were normalized using total cells protein. This is representative of n=5 independent experiments. (B-D) Effect of the knockdown of CD34 on the formation of tethers and slings on KG1a cells while rolling over E-selectin. Examples of the two-color fluorescence images of CD34 (cyan, immunostained by Alexa-Fluor-488-conjugated anti-CD34 antibody) and CD44 (yellow, immunostained by Alexa-Fluor-647-conjugated anti-CD44 antibody) on (B) control KG1a cell, (C) KG1a cell transfected with siRNA specific for CD34, and (D) KG1a cell transfected with scrambled control siRNA captured during cell rolling over the surface-deposited E-selectin molecules. The stained cells were injected into the microfluidic chambers whose surface was coated with rh E-selectin molecules at a density of 15 molecules μm^{-2}. The cells were injected into the chambers at a shear stress of 2 dyne cm^{-2}. These images were captured using identical imaging conditions and were shown in an identical image contrast.

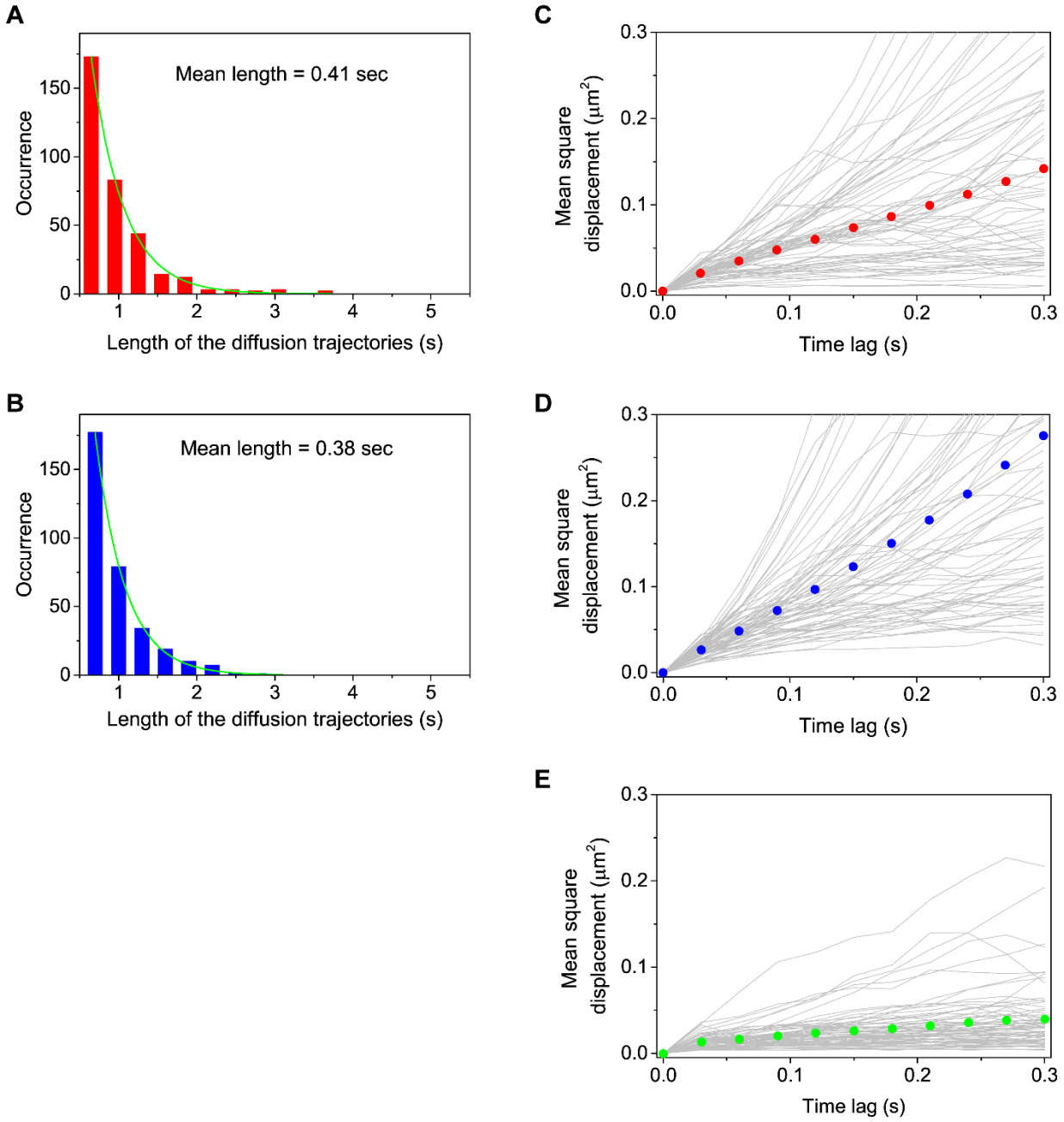

Figure S7. Single-molecule tracking analysis of PSGL-1 on KG1a cells. (A-B) Length of the single-molecule diffusion trajectories of the PSGL-1 molecules on the tethers and slings formed on KG1a cells rolling over E-selectin. Frequency histograms of the length of the single-molecule diffusion trajectories of PSGL-1 molecules (immunostained by Alexa-Fluor-555-conjugated anti-PSGL-1 antibody) that show diffusional motion on the (A) tethers and (B) slings formed during the KG1a cells rolling over E-selectin. The solid lines show the fitting to single-exponential decaying function. The mean trajectory lengths (0.41s and 0.38 s for the trajectories obtained from the tethers and slings, respectively) were calculated using the decay constants obtained by

the fits. The cells were injected into microfluidic chambers whose surface was coated with rh E-selectin molecules at a density of 15 molecules μm^{-2}. The cells were injected into the chambers at a shear stress of 2 dyne cm^{-2}. (C-D) MSD vs time-lag plots obtained from the single-molecule diffusion trajectories of PSGL-1 on the tethers and slings. MSD vs time-lag plots obtained for PSGL-1 molecules (immunostained by Alexa-Fluor-555-conjugated anti-PSGL-1 antibody) that show diffusional motion on the (C) tethers and (D) slings formed during KG1a cells rolling over E-selectin. The grey lines show individual MSD vs time-lag plots obtained from individual single-molecule diffusion trajectories. The red and blue dots show mean MSD vs time-lag plots for the tethers and slings, respectively. The cells were injected into microfluidic chambers whose surface was coated with recombinant E-selectin molecules at a density of 15 molecules μm^{-2}. The cells were injected into the chambers at a shear stress of 2 dyne cm^{-2}. (E) MSD vs time-lag plots obtained from the single-molecule diffusion trajectories of PSGL-1 localized on microvilli. MSD vs time-lag plots obtained for PSGL-1 molecules (immunostained by Alexa-Fluor-488-conjugated anti-PSGL-1 antibody) that are localized on microvilli in the control KG1a cells. The grey lines show individual MSD vs time-lag plots obtained from individual single-molecule diffusion trajectories. The green dots show mean MSD vs time-lag plot. The cells were injected into uncoated microfluidic chambers without any recombinant E-selectin molecules. The fluorescence images were captured in the absence of any external shear stress.

Captions for Supplemental Video 1 to 7

Video S1: Time-lapse fluorescence images of CD44 on a KG1a cell perfused into a microfluidic chamber at a shear stress of 1 – 8 dyne cm^{-2}. The CD44 molecules were immunostained by Alexa-Fluor-647-conjugated anti-CD44 antibody, clone 515. The surface of the microfluidic chamber was coated with rh E-selectin molecules at a density of 15 molecules μm^{-2}. Scale bar = 20 μm.

Video S2: Time-lapse fluorescence images of CD44 on a KG1a cell perfused into a microfluidic chamber that shows the conversion of a tether into sling. The CD44 molecules were immunostained by Alexa-Fluor-647-conjugated anti-CD44 antibody, clone 515. The cells were injected into the chambers at a shear stress of 6 dyne cm^{-2}. The surface of the microfluidic chamber was coated with rh E-selectin molecules at a density of 15 molecules μm^{-2}. Scale bar = 20 μm.

Video S3: Time-lapse fluorescence images of CD44 on a KG1a cell perfused into a microfluidic chamber that shows the retraction of the sling. The CD44 molecules were immunostained by Alexa-Fluor-647-conjugated anti-CD44 antibody, clone 515. The cells were injected into the chambers at a shear stress of 8 dyne cm^{-2}. The surface of the microfluidic chamber was coated with rh E-selectin molecules at a density of 15 molecules μm^{-2}. Scale bar = 20 μm.

Video S4: Time-lapse fluorescence images of PSGL-1 on a KG1a cell perfused into a microfluidic chamber that shows the discrete spatial distribution of the PSGL-1 molecules on the tether. The PSGL- molecules were immunostained by Alexa-Fluor-555-conjugated anti-PSGL-1 antibody, clone KPL-1. The cells were injected into the chambers at the shear stress of 2

dyne cm^{-2}. The surface of the microfluidic chamber was coated with rh E-selectin molecules at a density of 15 molecules μm^{-2}. Scale bar = 10 μm.

Video S5: Time-lapse fluorescence images of PSGL-1 on a KG1a cell perfused into a microfluidic chamber that shows the discrete spatial distribution of the PSGL-1 molecules on the sling. The PSGL- molecules were immunostained by Alexa-Fluor-555-conjugated anti-PSGL-1 antibody, clone KPL-1. The cells were injected into the chambers at a shear stress of 2 dyne cm^{-2}. The surface of the microfluidic chamber was coated with rh E-selectin molecules at a density of 15 molecules μm^{-2}. Scale bar = 10 μm.

Video S6: Time-lapse fluorescence images of CD44 on KG1a cells perfused into a microfluidic chamber that shows the formation of the tethers and slings on all the rolling cells. The CD44 molecules were immunostained by Alexa-Fluor-647-conjugated anti-CD44 antibody, clone 515. The cells were injected into the chambers at a shear stress of 4 dyne cm^{-2}. The surface of the microfluidic chamber was coated with rh E-selectin molecules at a density of 15 molecules μm^{-2}. Scale bar = 20 μm.

Video S7: Time-lapse fluorescence images of PSGL-1 on a KG1a cell perfused into a microfluidic chamber that shows the merger of multiple tethers. The PSGL- molecules were immunostained by Alexa-Fluor-555-conjugated anti-PSGL-1 antibody, clone KPL-1. The cells were injected into the chambers at a shear stress of 2 dyne cm^{-2}. The surface of the microfluidic chamber was coated with rh E-selectin molecules at a density of 15 molecules μm^{-2}. Scale bar = 5 μm.